bioRxiv preprint doi: https://doi.org/10.1101/2021.02.12.430913; this version posted February 12, 2021. The copyright holder for this preprint (which was not certified by peer review) is the author/funder, who has granted bioRxiv a license to display the preprint in perpetuity. It is made available under aCC-BY 4.0 International license.

KCTD19 associates with ZFP541 and HDAC1 and is required for meiotic exit in male mice

Seiya Oura[1,2],Takayuki Koyano[3], Chisato Kodera[4], Yuki Horisawa-Takada[4], Makoto Matsuyama[3], Kei-ichiro Ishiguro[4], and Masahito Ikawa[1,2,5 *]

[1] Research Institute for Microbial Diseases, Osaka University, Osaka, 565-0871, Japan

[2] Graduate School of Pharmaceutical Sciences, Osaka University, Osaka, 565-0871, Japan

[3] Division of Molecular Genetics, Shigei Medical Research Institute, Okayama, 701-0202, Japan

[4] Department of Chromosome Biology, Institute of Molecular Embryology and Genetics (IMEG), Kumamoto University, Kumamoto, 860-0811, Japan

[5] The Institute of Medical Science, The University of Tokyo, Minato-ku, Tokyo, 108-8639, Japan

[*]Correspondence: ikawa@biken.osaka-u.ac.jp (M. I.)

bioRxiv preprint doi: https://doi.org/10.1101/2021.02.12.430913; this version posted February 12, 2021. The copyright holder for this preprint (which was not certified by peer review) is the author/funder, who has granted bioRxiv a license to display the preprint in perpetuity. It is made available under aCC-BY 4.0 International license.

Abstract

Meiosis is a cell division process with complex chromosome events where various molecules must work in tandem. To find meiosis-related genes, we screened evolutionarily conserved and reproductive tract-enriched genes using the CRISPR/Cas9 system and identified potassium channel tetramerization domain containing 19 (*Kctd19*) as an essential factor for meiosis. In prophase I, *Kctd19* deficiency did not affect synapsis or the DNA damage response, and chiasma structures were also observed in metaphase I spermatocytes of *Kctd19* KO mice. However, spermatocytes underwent apoptotic elimination during the metaphase-anaphase transition. We were able to rescue the *Kctd19* KO phenotype with an epitope-tagged *Kctd19* transgene. Immunoprecipitation-mass spectrometry identified zinc finger protein 541 (ZFP541) and histone deacetylase 1 (HDAC1) as binding partners of KCTD19, indicating that KCTD19 is involved in chromatin modification. Phenotyping of *Zfp541* KO spermatocytes demonstrated XY chromosome asynapsis and recurrent DNA damage in the late pachytene stage, leading to apoptosis. In summary, our study reveals that KCTD19 associates with ZFP541 and HDAC1, and that both KCTD19 and ZFP541 were essential for meiotic exit in male mice.

bioRxiv preprint doi: https://doi.org/10.1101/2021.02.12.430913; this version posted February 12, 2021. The copyright holder for this preprint (which was not certified by peer review) is the author/funder, who has granted bioRxiv a license to display the preprint in perpetuity. It is made available under aCC-BY 4.0 International license.

Author summary

Meiosis is a fundamental process that consisting of one round of genomic DNA replication and two rounds of chromosome segregation producing four haploid cells. To properly distribute their genetic material, cells need to undergo complex chromosome events such as a physical linkage of homologous chromosomes (termed synapsis) and meiotic recombination. The molecules involved in these events have not been fully characterized yet, especially in mammals. Using a CRISPR/Cas9-screening system, we identified the potassium channel tetramerization domain containing 19 (*Kctd19*) as an essential factor for meiosis in male mice. Further, we identified zinc finger protein 541 (ZFP541) and histone deacetylase 1 (HDAC1) as binding partners of KCTD19. By observing meiosis of *Zfp541* knockout germ cells, we found that *Zfp541* was also essential for meiotic completion. These results show that the KCTD19/ZFP541 complex plays a critical role and is indispensable for male meiosis and fertility.

bioRxiv preprint doi: https://doi.org/10.1101/2021.02.12.430913; this version posted February 12, 2021. The copyright holder for this preprint (which was not certified by peer review) is the author/funder, who has granted bioRxiv a license to display the preprint in perpetuity. It is made available under aCC-BY 4.0 International license.

Introduction

Meiosis is a division process consisting of one round of DNA replication and two rounds of chromosome segregation, producing four haploid gametes. During meiotic prophase I, proteinaceous structures termed the synaptonemal complex (SC) are assembled on sister chromatids and form a scaffold along each homologous chromosome. The homologs begin to pair and synapse, followed by meiotic recombination yielding a physical tether between homologs (chiasmata). After completing these chromosome events, the cells transition to the first meiotic division, where homologs are segregated to the opposite poles followed by the segregation of sister chromatids in the next round of cell division.

The molecules involved in these complex chromosome events are not fully characterized yet, especially in mammals, due to difficulties in culturing and genetically manipulating spermatogenic cells in vitro. Thus, knockout (KO) of genes with testis-specific expression and evolutionarily conservation has been a powerful strategy to identify male meiosis-related genes and their functions (1). We have generated over 300 testis-enriched gene KO mice with conventional ES cell-mediated and the CRISPR/Cas9-mediated methods (2-5) and showed about one-third of them are indispensable for male fertility (6-8). During this phenotypic screening, we identified a potassium channel tetramerization domain containing 19 (*Kctd19*) as an evolutionarily conserved and testis expressed gene that is essential for male fertility in mice.

KCTD19 is one of 26 member KCTD family of proteins (9, 10) (KCTD1 – 21, KCTD12B, TNFAIP1, KCNRG, SHKBP1, and BTBD10; http://pfam.xfam.org/family/PF02214.22) which contains an N-terminal cytoplasmic tetramerisation domain (T1) usually found in voltage-gated potassium channels. The T1 domain is a subgroup of the BTB (Broad-complex, Tramtrack and Bric-à-brac) domain or

bioRxiv preprint doi: https://doi.org/10.1101/2021.02.12.430913; this version posted February 12, 2021. The copyright holder for this preprint (which was not certified by peer review) is the author/funder, who has granted bioRxiv a license to display the preprint in perpetuity. It is made available under aCC-BY 4.0 International license.

71 POZ (poxvirus and zinc finger) domain family, which are often found at the N-terminus of
72 C2H2-type zinc-finger transcription factors. A variety of biological functions have been
73 identified for KCTD proteins (10), including ion channel regulation (11, 12), apoptosis (13,
74 14), interaction with ubiquitin ligase complexes such as cullin 3 (CUL3) (15, 16), and
75 degradation of various proteins such as histone deacetylases (HDACs) (15, 17). Regarding
76 KCTD19, Choi *et al.* found that ZFP541 made complex with KCTD19 and HDAC1 in male
77 germ cells and valproic acid (HDAC inhibitor) treatment caused hyperacetylation and
78 KCTD19/ZFP541 reduction in round spermatids (18), suggesting that KCTD19/ZFP541 are
79 involved in chromatin reorganization during the post-meiotic phase (18).
80 In this study, we generated *Kctd19* KO mice using the CRISPR/Cas9 system and
81 revealed that *Kctd19* deficiency causes azoospermia due to incomplete meiosis.
82 Immunoprecipitation-mass spectrometry confirmed KCTD19, ZFP541, and HDAC1
83 interaction. Further, we also analyzed *Zfp541* null spermatocyte and showed that *Zfp541* is
84 necessary for pachytene exit. Our results suggested that KCTD19/ZFP541 complex
85 functions in chromatin modification during meiosis.
86

bioRxiv preprint doi: https://doi.org/10.1101/2021.02.12.430913; this version posted February 12, 2021. The copyright holder for this preprint (which was not certified by peer review) is the author/funder, who has granted bioRxiv a license to display the preprint in perpetuity. It is made available under aCC-BY 4.0 International license.

Results

Kctd19 is a testis-enriched and evolutionally conserved gene

To investigate the spatial expression of *Kctd19* in mice, we performed multi-tissue RT-PCR using cDNA obtained from adult tissues and embryonic ovary, and we found that *Kctd19* was specifically expressed in testis (Fig. 1A). In mice, the first wave of spermatogenesis starts soon after birth and completes within the first 35 days of postnatal development (19). To determine which stage of spermatogenic cells begin to express *Kctd19*, we also performed RT-PCR using cDNA obtained from postnatal testis as the first wave of spermatogenesis was progressing. The result shows that *Kctd19* expression starts around postnatal day (PND) 10 – 12 (Fig. 1B), which corresponds to the spermatocyte stage when the first wave of spermatogenesis reaches meiotic prophase. The PCR signals increased until PND 28 (Fig. 1B), at which time spermatid elongation starts.

The mouse KCTD19 protein comprises 950 amino-acid residues and has only one BTB domain based on SMART software (20) (Fig. 1C). Phylogenetic analysis with Clustal W2.1 (21) showed that KCTD19 was evolutionarily conserved in many mammals, including cattle, dogs, mice, and humans (Fig. 1D and S1). These results suggest that KCTD19 functions during the meiotic phase of mammalian spermatogenesis.

Kctd19 is required for male fertility.

To uncover the function of *Kctd19 in vivo*, we generated *Kctd19* KO mice using the CRISPR/Cas9 system. To avoid affecting the proximal genes, *Lrrc36* and *Plekhg4*, we designed the excision of the middle exons 3-12 from 16 exons total (Fig. 1E). Two crRNAs were mixed with tracrRNA and Cas9, and the prepared ribonucleoproteins (RNPs) were electroporated into murine zygotes. Of the 49 fertilized eggs that were electroporated, 40

bioRxiv preprint doi: https://doi.org/10.1101/2021.02.12.430913; this version posted February 12, 2021. The copyright holder for this preprint (which was not certified by peer review) is the author/funder, who has granted bioRxiv a license to display the preprint in perpetuity. It is made available under aCC-BY 4.0 International license.

two-cell embryos were transplanted into the oviducts of three pseudopregnant female mice. We obtained seven pups with the intended mutation. Subsequent mating and sequencing resulted in a heterozygous mouse with a 9620 bp deletion, referred to as *Kctd19*^{del} that were genotyped with PCR (Fig. 1F and G). We confirmed Kctd19 deletion with immunoblotting (Fig. 1H) with various antibodies raised against KCTD19 protein (see Fig. 1C). The results showed complete loss of KCTD19 in *Kctd19*$^{del/del}$ testis, and the antibodies specifically recognize KCTD19 (Fig. 1H). We used rabbit polyclonal antibody (pAb) and rat monoclonal antibody (mAb) #1 for immunoprecipitation, and rat mAb #2 for immunostaining in subsequent experiments.

Knockout (KO) mice obtained by heterozygous intercrosses showed no overt gross defects in development, behavior, and survival. We caged individual *Kctd19*$^{del/del}$ male mice with wild type (wt) females for two months to analyze their fertility. Although mating plugs were often observed, *Kctd19*$^{del/del}$ males failed to sire any pups (Fig. 1I). We observed normal numbers of pups from *Kctd19*$^{del/del}$ females with *Kctd19*$^{wt/del}$ males (7.8±2.2; Fig. 1J), indicating that *Kctd19* is not required for female fertility. As *Kctd19*$^{wt/del}$ male mice are fully fertile, we used littermate heterozygous males as controls in some experiments.

To determine if the BTB domain of KCTD19 is required for protein function, we removed exon 2 (297 bp) that encodes the BTB domain by designing two crRNAs targeting intron 1 and 2 (Fig. S2A – S2C). Despite generating an inframe mutation, the deletion of the BTB domain affected *Kctd19* expression or/and protein stability, and we could not detect any truncated KCTD19 protein with our antibodies (Fig. S2D and S2E). The exon 2 deleted mice showed the same phenotype as *Kctd19*$^{del/del}$ mice (Fig. S2F and 2C). Therefore, we regarded this Kctd19-ΔBTB line as equivalent to *Kctd19*$^{del/del}$ line, in that both lines result in male infertility, to corroborate that *Kctd19* is essential for male fertility.

bioRxiv preprint doi: https://doi.org/10.1101/2021.02.12.430913; this version posted February 12, 2021. The copyright holder for this preprint (which was not certified by peer review) is the author/funder, who has granted bioRxiv a license to display the preprint in perpetuity. It is made available under aCC-BY 4.0 International license.

135

136 **_Kctd19 del/del_ spermatocytes failed to complete meiosis.**

137 When we observed testis gross morphology, *Kctd19*$^{del/del}$ testis were smaller than
138 those of *Kctd19*$^{wt/del}$ (testis/ body weight: 4.5±0.2 x 10^{-3} [*wt/del*], 1.2±0.3 x 10^{-3} [*del/del*]; Fig.
139 2A and 2B), indicating defective spermatogenesis in *Kctd19*$^{del/del}$ testis. To define the cause
140 of testicular atrophy, we performed hematoxylin and periodic acid-Schiff (PAS) staining of
141 testicular sections. While three germ cell layers were seen in control testis sections, only two
142 layers of germ cells were observed in *Kctd19*$^{del/del}$ testis (Fig. 2C; low magnification). When
143 we compared testicular cells based on the cycle of the seminiferous epithelium (22) (23), the
144 nuclear morphology of spermatocytes was comparable between two genotypes up to
145 seminiferous stage X – XI, corresponding to the diplotene stage (Fig. 2C). In seminiferous
146 stage XII, spermatocytes proceeded to metaphase-anaphase in *Kctd19*$^{del/del}$ testis as well as
147 in *Kctd19*$^{wtl/del}$ testis (Fig. 2C). However, the *Kctd19*$^{del/del}$ spermatocytes could not complete
148 meiotic divisions and accumulated in tubules after stage XII (Fig. 2C; stage I – II). These
149 accumulated spermatocytes underwent apoptosis (Fig. 2D) and did not develop to haploid
150 spermatids. As a result, no mature spermatozoa were observed in the cauda epididymis
151 (Fig. 2E). These observations suggested that *Kctd19*$^{del/del}$ spermatocytes failed to complete
152 meiosis, leading to azoospermia.

153

154 **KCTD19 localized to the nuclei of prophase spermatocytes and round spermatids**

155 To determine KCTD19 localization, we performed immunostaining of testicular
156 sections with a specific antibody against KCTD19 (Rat mAb #2; Fig. 2F). KCTD19 signals
157 started to appear in the nuclei of spermatocytes in seminiferous stage III – IV (Fig. 2G),
158 corresponding to early pachytene stage. The signal continuously localized in the nuclei of

bioRxiv preprint doi: https://doi.org/10.1101/2021.02.12.430913; this version posted February 12, 2021. The copyright holder for this preprint (which was not certified by peer review) is the author/funder, who has granted bioRxiv a license to display the preprint in perpetuity. It is made available under aCC-BY 4.0 International license.

159 spermatocytes (Fig. 2G; stage VII – VIII and X – XI). During the metaphase-anaphase
160 transition in meiosis, KCTD19 signal spread throughout the cell (Fig. 2G; stage XII). The signals
161 remained in the nuclei of round spermatids after meiotic division and disappeared in elongating
162 spermatids. The KO phenotype and KCTD19 localization suggested that KCTD19 regulates
163 meiosis in spermatocyte nuclei.
164
165 **_Kctd19_$^{del/del}$ spermatocytes showed defects in metaphase I organization.**
166 Due to an apparent defect in meiosis in _Kctd19_$^{del/del}$ male mice, we examined DNA
167 double-strand breaks (DSBs) and synapsis by immunostaining γH2AX and synaptonemal
168 complex protein 3 (SYCP3), respectively. γH2AX signals appeared in the leptotene/zygotene
169 stage and disappeared in the pachytene/diplotene stage, except for the XY body (Fig. 3A
170 and 3B), suggesting that _Kctd19_ $^{del/del}$ spermatocytes underwent DSB initiation and resolution
171 as controls. Also, homologous chromosomes in _Kctd19_$^{del/del}$ spermatocytes synapsed in
172 pachytene stage and desynapsed in diplotene stage remaining physically connected at
173 chiasmata without obvious defects (Fig. 3A and 3B). However, the diplotene population
174 declined in juvenile _Kctd19_$^{del/del}$ males (P20), but not in adult males (Fig. 3C)
175 To uncover the cause of apoptosis in metaphase spermatocytes, we stained spread
176 chromosomes with Giemsa's staining. We observed a normal number of bivalent
177 chromosomes with chiasmata (Fig. 3D), consistent with immunostaining of prophase
178 spermatocytes. Next, we examined spindles in metaphase I spermatocytes by
179 immunostaining of CENPC and α-TUBULIN. Although _Kctd19_$^{del/del}$ spermatocytes formed
180 spindles without apparent defects, they showed chromosome misalignment (Fig. 3E and
181 3FF; WT: 0 %, *del/del*: 33 %). When we stained SYCP3, we observed SYCP3 aggregates
182 outside chromosomes, known as polycomplexes (24), more frequently in _Kctd19_$^{del/del}$ than in

bioRxiv preprint doi: https://doi.org/10.1101/2021.02.12.430913; this version posted February 12, 2021. The copyright holder for this preprint (which was not certified by peer review) is the author/funder, who has granted bioRxiv a license to display the preprint in perpetuity. It is made available under aCC-BY 4.0 International license.

183 WT metaphase spermatocytes (WT: 12 %, *del/del*: 65 %; Fig. 3G and 3H). These result
184 suggested that KCTD19 is required for metaphase I organization.
185
186 **An epitope-tagged transgene rescues the phenotype of *Kctd19*$^{del/del}$ mice**
187 To exclude the possibility that the observed phenotype in *Kctd19*$^{del/del}$ males was
188 caused by an off-target effect from CRISPR/Cas9 cleavage or an aberrant genetic
189 modification near the *Kctd19* locus, we carried out a rescue experiment by generating
190 transgenic (Tg) mouse lines. We mixed and injected two DNA constructs having 3xFLAG-
191 tagged *Kctd19* and 3xHA-tagged *Kctd19* under the testis-specific *Clgn* promoter (25) (Fig
192 4A) and established two Tg lines: one expressing only 3xHA-tagged *Kctd19* (Tg line #1) and
193 one expressing both 3xFLAG- and 3xHA-tagged *Kctd19* (Tg line #2; Fig 4B - D). When we
194 performed immunoprecipitation (IP) with Tg line #2, anti-FLAG antibody-conjugated beads
195 pull downed 3xHA-KCTD19, and vice versa (Fig. 4E and F), suggesting that KCTD19 is a
196 homomeric protein as previously reported (9, 26).
197 When we mated Tg positive *Kctd19*$^{del/del}$ male mice with superovulated WT female
198 mice (Fig. 4G), we could obtain 2-cell embryos from both Tg lines, #1 (Fig. 4H). In
199 *Kctd19*$^{del/del}$ mice carrying the 3xHA-*KCTD19* transgene (#1), the testicular size (testis/body
200 weight: 4.7 ± 1.6; Fig. 4J and 4K) was comparable to WT, and spermatogenesis evaluated
201 by HePAS staining looked normal. Further, with an anti-HA antibody, we observed a similar
202 immunostaining pattern with rat monoclonal anit-KCT19 (Fig. 2G), indicating that the 3xHA-
203 tag did not affect KCTD19 behavior and corroborated the immunostaining results with the
204 anti-KCTD19 antibody.
205
206 **KCTD19 assocaites with ZFP541 and HDAC1.**

bioRxiv preprint doi: https://doi.org/10.1101/2021.02.12.430913; this version posted February 12, 2021. The copyright holder for this preprint (which was not certified by peer review) is the author/funder, who has granted bioRxiv a license to display the preprint in perpetuity. It is made available under aCC-BY 4.0 International license.

To elucidate KCTD19 function, we identified interacting proteins by immunoprecipitation (IP) and mass spectrometry (MS). We lysed *Kctd19*$^{del/del}$ and juvenile (PND21) WT testis with non-ionic detergent (NP40) and incubated the lysate with antibodies (rabbit pAb and rat mAb #1) and protein G-conjugate beads. The specific co-IPed proteins were visualized by SDS-PAGE and silver staining (Fig. 5A and B). When eluted samples were subjected to MS analysis, HDAC1 (histone deacetylase 1) and ZNF541 (Zinc finger protein 54; ZFP541) were reproducibly detected with both antibodies (Fig. 5C), consistent with a prior study (18). KCTD19 and HDAC1 association was confirmed by reciprocal IP with an anti-HDAC1 antibody (Fig. 5D).

HDAC1 is a modulator of chromatin structure and disruption of HDAC1 results in embryonic lethality before E10.5 (27) In previous reports, KCTDs were implicated in HDAC degradation (15, 17). We examine the behavior of HDAC1 in *Kctd19*$^{del/del}$ testis by immunoblotting analysis and immunostaining with the anti-HDAC1 antibody. HDAC1 protein levels and localization were comparable between *Kctd19*$^{del/del}$ and WT testis (Fig. 5E and 5F). The HDAC1 staining intensity was the strongest in spermatocytes in stage X – XI and lost in elongating spermatids (Fig. 5F), reminiscent of the KCTD19 staining pattern (Fig. 2G). These results indicated that KCTD19 works together with HDAC1 in regulating meiotic exit.

Zfp541 deficient spermatocytes fail to exit the pachytene stage.

The second factor identified by co-IP MS analysis, *Zfp541*, is evolutionally conserved (Fig. S3) and specifically expressed in testis (Fig. 6A). Further, the expression begins around PND10 – 12 and was then continuously detected with increasing signal intensity at PND 28 (Fig. 6B), reminiscent of *Kctd19* rtPCR (Fig. 1B). The mouse ZFP541 protein comprises 1363 amino-acid residues and has five C2H2 type zinc finger motifs, one

bioRxiv preprint doi: https://doi.org/10.1101/2021.02.12.430913; this version posted February 12, 2021. The copyright holder for this preprint (which was not certified by peer review) is the author/funder, who has granted bioRxiv a license to display the preprint in perpetuity. It is made available under aCC-BY 4.0 International license.

231 ELM2 domain, and one SANT domain based on SMART software (20), indicating
232 KCTD19/ZFP541 binds DNA. To reveal the function of ZFP541 and its relationship with
233 KCTD19, we analyzed *Zfp541* KO phenotype with chimeric mice (chimeric analysis) (4) (5).
234 To disrupt gene function completely and minimize an effect on a juxtapose gene,
235 *Napa*, we designed two sgRNAs targeting the sequence upstream of the start codon and
236 intron 8 (Fig 6C), and transfected embryonic stem (ES) cells expressing EGFP (28) with two
237 pairs of sgRNA/Cas9 expressing plasmids (pair 1: gRNA 1 and 3; pair 2: gRNA 2 and 4; Fig
238 6C). We Screened 32 clones for each pair, and obtained 13 and 11 mutant clones with
239 biallelic deletion for pair 1 and 2. Accounting for ES cell quality and off-target cleavages, we
240 produced chimeric mice with one ES cell clone from pair 1 (1 – 3 #2) and pair 2 (2 – 4 #3)
241 (Fig 6D and E).
242 First, we examined spermatogenesis with HePAS staining of testicular sections.
243 Almost no round spermatids with GFP were observed in chimeric mice (Fig 6F), as seen in
244 *Kctd19*$^{del/del}$ testis sections. *Zfp541* deficient spermatocytes were eliminated by apoptosis in
245 stage X – XII seminiferous tubules without reaching metaphase (Fig 6G). Next, we
246 performed immunostaining with the antibodies against KCTD19. The KCTD19 intensity
247 became weaker, although not lost, in the nuclei of *Zfp541* deficient spermatocytes than that
248 of adjacent WT spermatocytes (Fig 6H). On the other hand, the immunofluorescence
249 intensity of HDAC1 was comparable between *Zfp541* deficient and WT spermatocytes (Fig
250 6I). Finally, we examined the DNA damage response and synapsis in a XX/XY (Host/ES)
251 chimeric male mouse (29), in which all spermatocytes are derived from the mutant ES cells
252 (Fig. S4A and S4B). *Zfp541* deficient spermatocytes initiated DSBs in the leptotene/zygotene
253 stage and resolved the breaks in the early pachytene stage (Fig. 6J). However, late
254 pachytene spermatocytes showed recurrent DSBs. Further, when we meticulously examined

bioRxiv preprint doi: https://doi.org/10.1101/2021.02.12.430913; this version posted February 12, 2021. The copyright holder for this preprint (which was not certified by peer review) is the author/funder, who has granted bioRxiv a license to display the preprint in perpetuity. It is made available under aCC-BY 4.0 International license.

255 early pachytene spermatocytes, we could observe asynapsis of XY chromosomes (red and
256 yellow boxes in Fig. 4J). No diplotene spermatocytes were observed in the chimeric mouse,
257 consistent with histological analysis. Collectively, these results showed that *Zfp541* deficient
258 spermatocytes did not reach the diplotene stage. Thus, KCTD19 may function downstream
259 of ZFP541.
260

bioRxiv preprint doi: https://doi.org/10.1101/2021.02.12.430913; this version posted February 12, 2021. The copyright holder for this preprint (which was not certified by peer review) is the author/funder, who has granted bioRxiv a license to display the preprint in perpetuity. It is made available under aCC-BY 4.0 International license.

Discussion

In the present study, we identified *Kctd19* as a male fertility-related factor by CRISPR/Cas9-mediated screening of testis enriched genes and validated our result with transgenic rescue experiments. Recently, Fang *et al.* also reported metaphase I arrest in *Kctd19* KO male mice (30), corroborating our results. In detailed phenotypic analyses, we found that *Kctd19* KO spermatocytes failed to complete meiotic division with defects in metaphase I organization. Further, we revealed that KCTD19 associates with ZFP541 and HDAC1 by co-IP experiment using two antibodies against KCTD19. Finally, we produced chimeric mice with *Zfp541*-KO ES cells and showed that *Zfp541* is essential for pachytene exit.

Kctd19 KO spermatocytes showed a metaphase-anaphase arrest and were eliminated by apoptosis. One of the most frequent causes of metaphase I arrest is crossover (CO) defect causing precocious homolog segregation (31, 32). However, *Kctd19* KO spermatocytes had a normal number of bivalents (20 homologs) in metaphase I, indicating that homologs were physically connected in *Kctd19* KO spermatocytes. We also observed SYCP3 polycomplexes (24), alternative SC structures, in metaphase I spermatocytes. A common cause of synaptonemal polycomplex formation is an excess amount of free SC components (24), which might be caused by premature dissociation of SC or misregulation of SC-related protein expression. However, we could not rule out the possibility that these metaphase I structural defects might be a secondary effect or phenomena in dying cells. In addition, we observed a delay of metaphase entry or elimination during prophase I in juvenile *Kctd19* KO males (PND20), indicating that KCTD19 may function also during prophase or that the first wave of spermatogenesis is exceptional.

bioRxiv preprint doi: https://doi.org/10.1101/2021.02.12.430913; this version posted February 12, 2021. The copyright holder for this preprint (which was not certified by peer review) is the author/funder, who has granted bioRxiv a license to display the preprint in perpetuity. It is made available under aCC-BY 4.0 International license.

To clarify the molecular function of KCTD19, we tried to identify interacting proteins by IP-MS analysis and found ZFP541 and HDAC1 as candidate proteins, consistent with the previous report (18). Although some KCTD members have been reported to be associated with HDAC degradation, we could not observe HDAC1 reduction in KCTD19 KO testis by immunoblotting or immunostaining analysis. On the other hand, the KCTD19/ZFP541 complex is reminiscent of BTB-ZF proteins, which have another subset of the BTB domain and the Krüppel-type C2H2 zinc fingers (33). Many BTB-ZF proteins have been implicated in transcriptional repressors such as N-CoR, SMRT, and HDACs via the BTB domain (34, 35) (36). The ELM2-SANT domain included in ZFP541 has also been shown to interact with HDAC1 (18, 37-39). Combined with these previous reports, our results suggested that the KCTD19/ZFP541 complex works on chromatin modification of spermatocytes with HDAC1. We also detected CUL9 and DNTTIP1 in the IP-MS analysis with rabbit-generated anti-KCTD19 antibody, albeit not with the rat antibody. These factors can be excellent targets in future research because knockdown experiments from other groups showed that CUL9 protects mouse eggs from aneuploidy (40) and DNTTIP1 loss causes chromosome misalignment in mitosis (41).

Finally, the chimeric analysis showed that *Zfp541* KO spermatocytes failed to exit the pachytene stage, unlike *Kctd19* KO spermatocytes underwent apoptosis during the metaphase-anaphase transition. *Zfp541* KO spermatocytes failed XY chromosome synapsis, and γH2AX foci signals regained outside the XY body in the late pachytene stage, resulting in apoptosis. Again, we acknowledge that these pachytene structural defects might be secondary effects or phenomena in dying cells.

In summary, our results showed that KCTD19 associates with ZFP541 and HDAC1 and are essential for meiotic exit. Further comparable studies will unveil the exact functions

bioRxiv preprint doi: https://doi.org/10.1101/2021.02.12.430913; this version posted February 12, 2021. The copyright holder for this preprint (which was not certified by peer review) is the author/funder, who has granted bioRxiv a license to display the preprint in perpetuity. It is made available under aCC-BY 4.0 International license.

of KCTD19 and ZFP541, which will give some insight into the molecular mechanism in male meiosis.

Materials and methods

Animals

All animal experiments were approved by the Animal Care and Use Committee of the Research Institute for Microbial Diseases, Osaka University (#Biken-AP-H30-01). Animals were housed in a temperature-controlled environment with 12 h light cycles and free access to food and water. B6D2F1 (C57BL/6 × DBA2; Japan SLC, Shizuoka, Japan) mice and ICR (SLC) were used as embryo donors; B6D2F1 were used for mating and wild-type control; C57BL6/N (SLC) mice were used to collect RNA for RT-PCR and cloning. Gene-manipulated mouse lines used in this study will be deposited at both the Riken BioResource Center (Riken BRC, Tsukuba, Japan) and the Center for Animal Resources and Development, Kumamoto University (CARD, Kumamoto, Japan). All lines are available through these centers.

Egg collection

To prepare eggs for knockout mouse production, female mice were superovulated by injection of CARD HyperOva (0.1 mL, Kyudo, Saga, Japan) into the abdominal cavity of B6D2F1 females, followed by injection of human chorionic gonadotropin (hCG) (7.5 units, ASKA Pharmaceutical, Tokyo, Japan). Natural mating was done with B6D2F1 males 46~48 h after CARD HyperOva injection. After 19-21 h, cumulus-intact eggs were collected and treated with 0.33 mg/mL hyaluronidase (Wako, Osaka, Japan) for 5 min to remove cumulus

bioRxiv preprint doi: https://doi.org/10.1101/2021.02.12.430913; this version posted February 12, 2021. The copyright holder for this preprint (which was not certified by peer review) is the author/funder, who has granted bioRxiv a license to display the preprint in perpetuity. It is made available under aCC-BY 4.0 International license.

331 cells for genome editing. Obtained eggs were cultured in KSOM medium at 37℃ under 5%
332 CO2 until subsequent treatments.
333
334 ***Generation of Kctd19 deletion and Kctd19-ΔPOZ/TAZ mice***
335 *Kctd19* deletion mice and *Kctd19*-ΔPOZ/TAZ mice were generated by electroporation
336 described previously (42, 43). Briefly, a gRNA solution was prepared by annealing two
337 tracrRNAs (Sigma-Aldrich, St. Louis, MO, USA) and crRNA (Sigma-Aldrich). The target
338 genomic sequences are listed in Table S1. Then, the gRNA solution and Cas9 nuclease
339 solution (Thermo Fisher Scientific, Waltham, MA, USA) were mixed. The final concentrations
340 of gRNA and Cas9 were as follows: for pronuclear injection, 20 ng/μL gRNA, and 100 ng/μL
341 Cas9 nucleases. The obtained complex was electroporated into fertilized eggs using a
342 NEPA21 electroporator (NEPA GENE, Chiba, Japan). The electroporated eggs were
343 transplanted into the oviduct ampulla of pseudopregnant mice (ICR; 10 embryos per ampulla)
344 on the following day. After 19 days, pups were delivered through Caesarean section and
345 placed with foster mothers (ICR). To generate heterozygous mutant mice, F0 mice were mated
346 with WT B6D2F1. Mouse colonies with a 9612 bp deletion and a 2172 bp deletion were
347 maintained by sibling mating and used for the phenotype analysis of *Kctd19* deletion and
348 *Kctd19*-ΔPOZ, respectively. The genotyping primers (GeneDesign, Osaka, Japan) and
349 amplification conditions are available in Table S1.
350
351 **Generation of 3xFLAG-*Kctd19* and *Kctd19*-3xHA transgenic mice**
352 The mouse *Kctd19* cDNA (ENSMUST00000167294.7) was tagged 3xFLAG or 3xHA
353 tag with a rabbit polyA signal inserted under the control of the mouse Clgn promoter. After
354 linearization, an equal amount of the DNA constructs (2.16 ng/μL; 0.54 ng/μL/kbp) were mixed

bioRxiv preprint doi: https://doi.org/10.1101/2021.02.12.430913; this version posted February 12, 2021. The copyright holder for this preprint (which was not certified by peer review) is the author/funder, who has granted bioRxiv a license to display the preprint in perpetuity. It is made available under aCC-BY 4.0 International license.

and injected into the pronucleus of fertilized eggs. The injected eggs were transplanted into the oviduct ampulla of pseudopregnant mice (ICR; 10 embryos per ampulla) the following day. After 19 days, pups were delivered through Caesarean section and placed with foster mothers (ICR). Offspring carrying both the 3xFLAG tag-*Kctd19* and *Kctd19*-3xHA transgenes and mice carrying only 3xHA tag-*Kctd19* transgene were used in this study. The genotyping primers (GeneDesign) are available in Table S1.

Generation of *Zfp541* KO ES cells and chimeric mice.

Zfp541 KO embryonic stem (ES) cells were generated using methods previously described (5). Briefly, EGR-G01 ES cells were transfected with two pX459 plasmids (Addgene plasmid #62988) with the target sequences (Table S1), and colonies were selected after transient puromycine selection. ES cells with normal karyotypes were injected into ICR embryos and chimeric blastocysts were transferred into the uteri of pseudopregnant females to produce chimeric offspring. Chimeric mals with high ES cell contribution were used for experiments.

Cell Lines

EGR-G01 ES cells were generated in the Ikawa Lab (28) and cultured in KnockOut DMEM (108297-018, Thermo Fisher Scientific) supplemented with 1% Penicillin-Streptomycin- Glutamine, 55 μM 2-mercaptoethanol, 1% Non-Essential Amino Acid Solution (11140-050, Thermo Fisher Scientific), 1% Sodium Pyruvate (11360-070, Thermo Fisher Scientific), 30 μM Adenosine (A4036, Sigma- Aldrich, St. Louis, MO, USA), 30 μM Guanosine (G6264, Sigma-Aldrich), 30 μM Cytidine (C4654, Sigma-Aldrich), 30 μM Uridine

bioRxiv preprint doi: https://doi.org/10.1101/2021.02.12.430913; this version posted February 12, 2021. The copyright holder for this preprint (which was not certified by peer review) is the author/funder, who has granted bioRxiv a license to display the preprint in perpetuity. It is made available under aCC-BY 4.0 International license.

(U3003, Sigma-Aldrich), 10 μM Thymidine (T1895, Sigma-Aldrich), 100 U/ml mouse LIF, and 20% FCS (51650-500, Biowest, Nuaillé, France).

Bacterial strains

Escherichia coli (*E. coli*) strain DH5α (Toyobo, Osaka, Japan) and BL21(de3) pLysS (C606003, ThermoFisher Scientific) were used for DNA cloning and protein expression, respectively. *E. coli* cells were grown in LB or 2×YT medium containing 100 mg/L ampicillin and were transformed or cloned using standard methods.

Production of antibodies against KCTD19

A polyclonal antibody against mouse KCTD19 was generated by immunizing rabbits with the synthetic peptide KRAITLKDWGKQRPKDRES corresponding to amino acids 747-765 of mouse KCTD19 (NP_808459.1). For monoclonal antibody production, the DNA encoding mouse KCTD19 (residue 654-793 aa, NP_808459.1) was inserted into pGEX6p-1 (GE healthcare), and the expression vector was transformed into *E. coli* strain BL21 (de3) pLysS (C606003, Thermo Fisher Scientific). GST-KCTD19 was purified using Glutathione Sepharose 4B (GE Healthcare). The purified KCTD19 protein with a complete adjuvant was injected into female rats. After 17 days of injection, lymphocytes were collected from iliac lymph nodes and hybridomas were generated (44, 45). The cell clones were screened by limited dilution.

Sequence comparison analysis

Amino acid sequences of KCTD19 and ZFP541 were obtained from the NCBI Entrez Protein database. Clustal W2.1 was used for multiple sequence alignment (21).

bioRxiv preprint doi: https://doi.org/10.1101/2021.02.12.430913; this version posted February 12, 2021. The copyright holder for this preprint (which was not certified by peer review) is the author/funder, who has granted bioRxiv a license to display the preprint in perpetuity. It is made available under aCC-BY 4.0 International license.

402

403 ***RT-PCR***

404 Using TRIzol reagent (15596-018, ThermoFisher Scientific), total RNA was isolated
405 from multiple adult tissues of C57BL6/N mice, testes ranging from 1 to 35-day-old mice, and
406 embryonic ovaries of PND 11.5-19.5. cDNAs were prepared using SuperScript IV Reverse
407 Transcriptase (180-90050, ThermoFisher Scientific) following the manufacturer's instructions.
408 Polymerase chain reaction (PCR) was performed using KOD Fx neo (KFX-201, TOYOBO,
409 Osaka, Japan). The primers (GeneDesign) and amplification conditions for each gene are
410 summarized in Table S1.

411

412 ***Genotype analysis***

413 PCR was performed using KOD FX neo (KFX-201, TOYOBO). The primers
414 (GeneDesign) and amplification conditions for each gene are summarized in Table S1. PCR
415 products were purified using a Wizard SV Gel and PCR Clean-Up System (Promega, Madison,
416 WI, USA) kit, and Sanger sequenced was done using sequence primers listed in Table S1.

417

418 ***Fertility analysis of KO mice***

419 To examine fertility, sexually mature male mice were housed with wild-type females
420 (B6DF1) for at least three months. Both plug and pup numbers were recorded at approximately
421 10 AM to determine the number of copulations and litter size.

422

423 ***Immunoblotting***

424 Proteins from testis were extracted using NP40 lysis buffer [50mM Tris-HCl (pH 7.5),
425 150 mM NaCl, 0.5% NP-40, 10% Glycerol]. Proteins were separated by SDS-PAGE under

bioRxiv preprint doi: https://doi.org/10.1101/2021.02.12.430913; this version posted February 12, 2021. The copyright holder for this preprint (which was not certified by peer review) is the author/funder, who has granted bioRxiv a license to display the preprint in perpetuity. It is made available under aCC-BY 4.0 International license.

426 reducing conditions and transferred to polyvinylidene fluoride (PVDF) membrane using the
427 Trans Blot Turbo system (BioRad, Munich, Germany). After blocking with 10% skim milk
428 (232100, Becton Dickinson, Cockeysville, MD, USA), the membrane was incubated with
429 primary antibody overnight at 4°C, and then incubated with HRP-conjugated secondary
430 antibody for 1 h at room temperature. Chemiluminescence was detected by ECL Prime
431 Western Blotting Detection Reagents (RPN2232, GE Healthcare, Chicago, IL, USA) using the
432 Image Quant LAS 4000 mini (GE Healthcare). The antibodies used in this study are listed in
433 Table S2.
434
435 **Morphological and histological analysis of testis**
436 To observe testis gross morphology and measure testicular weight, 11-12 week-old
437 male mice were euthanized after measuring their body weight. The whole testis was observed
438 using BX50 and SZX7 (Olympus, Tokyo, Japan) microscopes. For histological analysis, testes
439 were fixed with Bouin's fixative (16045-1, Polysciences, Warrington, PA, USA) at 4°C O/N,
440 dehydrated in increasing ethanol concentrations and 100% xylene, embedded in paraffin, and
441 sectioned (5 μm). The paraffin sections were hydrated with Xylene and decreasing ethanol
442 concentrations and treated with 1% periodic acid (26605-32, Nacalai Tesque, Kyoto, Japan)
443 for 10 min, treated with Schiff's reagent (193-08445, Wako) for 20 min, counterstained with
444 Mayer's hematoxylin solution (131-09665, Wako) for 3 min, dehydrated in increasing ethanol
445 concentrations, and finally mounted with Permount (SP15-100-1, Ferma, Tokyo, Japan). The
446 sections were observed using a BX53 (Olympus) microscope.
447
448 ***Apoptosis detection in testicular section***
449 TdT-mediated dUTP nick end labeling (TUNEL) staining was carried out with In Situ

bioRxiv preprint doi: https://doi.org/10.1101/2021.02.12.430913; this version posted February 12, 2021. The copyright holder for this preprint (which was not certified by peer review) is the author/funder, who has granted bioRxiv a license to display the preprint in perpetuity. It is made available under aCC-BY 4.0 International license.

Apoptosis Detection Kit (MK500, Takara Bio Inc., Shiga, Japan), according to the manufacturer's instruction. Briefly, testes were fixed with Bouin's fixative, embedded in paraffin, and sectioned (5 μm). After paraffin removal, the slides were boiled in citrate buffer (pH 6.0; 1:100; ab93678, abcam, Cambridge, UK) for 10 min and incubated in 3% H_2O_2 at room temperature for 5 min for endogenous peroxidase inactivation, followed by a labeling reaction with TdT enzyme and FITC-conjugated dUTP at 37°C for 1 h.

For chromogenic detection of apoptosis, the sections were incubated with HRP-conjugated anti-FITC antibody at 37°C for 30 min. The section was then incubated in ImmPACT DAB (SK-4105, Vector Laboratories, Burlingame, CA, USA) working solution, counterstained with Mayer's hematoxylin solution for 3 min, dehydrated in increasing ethanol concentrations, and finally mounted with Permount. The sections were observed using a BX53 (Olympus) microscope.

Immunostaining of testes

Testes were fixed in 4% paraformaldehyde (PFA) overnight at 4 °C, followed by dehydration in increasing ethanol concentrations and 100% of xylene, embedded in paraffin, and sectioned (5 μm). After paraffin removal, the slides were boiled in pH 6.0 citrate buffer for 10 min, blocked and permeabilized in 10% goat serum and 0.1% TritonX-100 for 20 min in PBS, and incubated with primary antibody overnight at 4°C or 1 h at room temperature in blocking solution; 1 h incubation was performed when using rat monoclonal anti-KCTD19 antibody. After incubation with AlexaFlour488/546-conjugated secondary antibody (1:200) at room temperature for 1 h, samples are counterstained with Hoechst 33342 (1:2000; H3570, Thermo Fisher Scientific) and mounted with Immu-Mount (9990402, Thermo Fisher Scientific). The antibodies used in this study are listed in Table S2.

bioRxiv preprint doi: https://doi.org/10.1101/2021.02.12.430913; this version posted February 12, 2021. The copyright holder for this preprint (which was not certified by peer review) is the author/funder, who has granted bioRxiv a license to display the preprint in perpetuity. It is made available under aCC-BY 4.0 International license.

Seminiferous tubule stages were identified based on the morphological characteristics of the germ cell nuclei and acrosome staining with AlexaFlour488/568-conjugated lectin PNA (L21409/L32458, Thermo Fisher Scientific). The sections were observed using a BX53 (Olympus) microscope and a Nikon Eclipse Ti microscope connected to a Nikon C2 confocal module (Nikon, Tokyo, Japan). Fluorescent images were false-colored and cropped using ImageJ software.

Immunostaining of surface chromosome spread

Spread nuclei from spermatocytes were prepared as described (46) with slight modification. In brief, seminiferous tubules were unraveled using forceps in ice-cold DMEM (11995065, Thermo Fisher Scientific) and incubated in 1 mg/mL collagenase (C5138, Sigma-Aldrich) in DMEM (20 mL) at 37°C for 15 min. After 3 washes with DMEM, the tubules were transferred to 20 mL trypsin/DNaseI medium [0.025 w/v% trypsin, 0.01 w/v% EDTA, 10U DNase in DMEM] and incubated at 37 °C for 10 min. After adding 5 mL of heat-inactivated FCS and pipetting, the solution was filtered through 59 µm mesh (N-N0270T, NBC Meshtec inc., Tokyo, Japan) to remove tubule debris. The collected testicular cells were resuspended in hypotonic solution [100 mM sucrose] and 10µL of the suspension was dropped onto a slide glass with 100 µL of fixative solution [100 µL of 1% PFA, 0.1% (v/v) Triton X-100]. The slides were then air-dried and washed with PBS containing 0.4% Photo-Flo 200 (1464510, Kodak Alaris, NY, USA) or frozen for longer storage at -80ºC.

The spread samples were blocked with 10% goat serum in PBS and then incubated with primary antibodies overnight at 4°C in blocking solution. After incubation with AlexaFlour 488/546-conjugated secondary antibody (1:200) at room temperature for 1 h, samples are counterstained with Hoechst 33342 and mounted with Immu-Mount. The samples were

bioRxiv preprint doi: https://doi.org/10.1101/2021.02.12.430913; this version posted February 12, 2021. The copyright holder for this preprint (which was not certified by peer review) is the author/funder, who has granted bioRxiv a license to display the preprint in perpetuity. It is made available under aCC-BY 4.0 International license.

observed using a BX53 (Olympus) microscope.

Giemsa staining of metaphase I chromosome spread

For preparing metaphase chromosome spreads, seminiferous tubules were unraveled using forceps in ice-cold PBS and transferred to a 1.5-mL tube with 1 mL of accutase (12679-54, Nacalai Tesque), followed by clipping the tubules, and a 5 min incubation at room temperature. After filtration with a 59 μm mesh and centrifugation, the cells were resuspended in 8 mL of hypotonic solution [1% sodium citrate] and incubated for 5 min at room temperature. The suspension was centrifuged and 7 mL of supernatant was aspirated. The cells were then resuspended in the remaining 1 mL of supernatant and 7 mL of Carnoy's Fixative (75 % Methanol, 25% Acetic Acid) were added gradually while shaking. After 2 washes with Carnoy's Fixative, the cells were resuspended ~ 0.5 mL of Carnoy's Fixative and dropped onto a wet glass slide. The slide was stained with Giemsa Stain Solution (079-04391, wako) and observed using a BX53 (Olympus) microscope.

Immunostaining of metaphase I cells

For cytological analysis of metaphase I cells, seminiferous tubule squashes were performed as previously described (47). In brief, seminiferous tubules were incubated in fix/lysis solution [0.1 % TritonX-100, 0.8 % PFA in PBS] at room temperature for 5 min. Tubule bunches were then put on glass slides with 100 μL of fix/lysis solution, minced into 1.0 ~ 3.0 mm segments with forceps, and arranged so that no tubule segment overlaped. After removing the excess amount of fix/lysis solution, a coverslip and pressure was applied to disperse cells, followed by flash freezing in liquid nitrogen for 15 sec, and removing the coverslip with forceps and a needle. For longer storage, the slide glasses were kept at -80 ºC with the coverslip.

bioRxiv preprint doi: https://doi.org/10.1101/2021.02.12.430913; this version posted February 12, 2021. The copyright holder for this preprint (which was not certified by peer review) is the author/funder, who has granted bioRxiv a license to display the preprint in perpetuity. It is made available under aCC-BY 4.0 International license.

The slides were blocked and permeabilized in 10% goat serum and 0.1% Triton X-100 for 20 min in PBS, and incubated with primary antibody overnight at 4°C. After incubation with AlexaFlour 488/546-conjugated secondary antibody (1:200) at room temperature for 1 h, samples are counterstained with Hoechst 33342 (1:2000) and mounted with Immu-Mount. Z-stack images were taken using a BZ-X700 (kyence, Osaka, Japan) microscope and stacked using ImageJ software. The antibodies used in this study are listed in Table S2.

Immunoprecipitation and mass spectrometry analysis

Proteins from testis were extracted using NP40 lysis buffer [50 mM Tris-HCl (pH7.5), 150 mM NaCl, 0.5% NP-40, 10% Glycerol]. Protein lysates were mixed with Dynabeads Protein G (Thermo)-conjugated with 2.0 μg of antibody. The immune complexes were incubated for 1 h at 4°C and washed 3 times with NP40 lysis buffer. Co-immunoprecipitated products were then eluted with 18 μL of 100 mM Gly-HCl (pH2.5) and neutralized with 2μL of 1 M Tris. The antibodies used in this study are listed in Table S2. Half of the eluted amount was subjected to SDS-PAGE and silver staining (06865-81, Nacalai Tesque). The remaining half amount was subjected to mass spectrometry (MS) analysis.

The proteins were reduced with 10 mM dithiothreitol (DTT), followed by alkylation with 55 mM iodoacetamide, and digested by treatment with trypsin and purified with a C18 tip (GL-Science, Tokyo, Japan). The resultant peptides were subjected to nanocapillary reversed-phase LC-MS/MS analysis using a C18 column (25 cm × 75 um, 1.6 μm; IonOpticks, Victoria, Australia) on a nanoLC system (Bruker Daltoniks, Bremen, Germany) connected to a tims TOF Pro mass spectrometer (Bruker Daltoniks) and a modified nano-electrospray ion source (CaptiveSpray; Bruker Daltoniks). The mobile phase consisted of water containing 0.1% formic acid (solvent A) and acetonitrile containing 0.1% formic acid (solvent B). Linear gradient elution

bioRxiv preprint doi: https://doi.org/10.1101/2021.02.12.430913; this version posted February 12, 2021. The copyright holder for this preprint (which was not certified by peer review) is the author/funder, who has granted bioRxiv a license to display the preprint in perpetuity. It is made available under aCC-BY 4.0 International license.

was carried out from 2% to 35% solvent B for 18 min at a flow rate of 400 nL/min. The ion spray voltage was set at 1.6 kV in the positive ion mode. Ions were collected in the trapped ion mobility spectrometry (TIMS) device over 100 ms and MS and MS/MS data were acquired over an *m/z* range of 100-1,700. During the collection of MS/MS data, the TIMS cycle was adjusted to 1.1 s and included 1 MS plus 10 parallel accumulation serial fragmentation (PASEF)-MS/MS scans, each containing on average 12 MS/MS spectra (>100 Hz), and nitrogen gas was used as the collision gas.

The resulting data were processed using DataAnalysis version 5.1 (Bruker Daltoniks), and proteins were identified using MASCOT version 2.6.2 (Matrix Science, London, UK) against the SwissProt database. Quantitative value and fold exchange were calculated by Scaffold4 (Proteome Software, Portland, OR, USA) for MS/MS-based proteomic studies.

Chimeric analysis

For distinguishing ESC-derived germ cells, GFP was stained by immunofluorescence or immunohistochemistry. The antibodies used in this study are listed in Table S2.

Author contributions

S.O. and M.I. conceived and designed the research; S.O. performed experiments; S.O., T.K, C.K, Y.T., and K.I prepared materials; S.O. analyzed data; S.O. and M.I. wrote the paper.

Declaration of interests

The authors declare no competing interests.

bioRxiv preprint doi: https://doi.org/10.1101/2021.02.12.430913; this version posted February 12, 2021. The copyright holder for this preprint (which was not certified by peer review) is the author/funder, who has granted bioRxiv a license to display the preprint in perpetuity. It is made available under aCC-BY 4.0 International license.

570 **Data availability statement**

571 The authors declare that the data that support the findings of this study are

572 available from the corresponding author upon request.

573

bioRxiv preprint doi: https://doi.org/10.1101/2021.02.12.430913; this version posted February 12, 2021. The copyright holder for this preprint (which was not certified by peer review) is the author/funder, who has granted bioRxiv a license to display the preprint in perpetuity. It is made available under aCC-BY 4.0 International license.

Acknowledgement

We would like to thank Eri Hosoyamada and Mei Koyama for their technical assistance and Dr. Julio M. Castaneda for the critical reading of the manuscript. This work was supported by the Ministry of Education, Culture, Sports, Science and Technology (MEXT)/Japan Society for the Promotion of Science (JSPS) KAKENHI grants (JP19J21619 to S.O., JP19H05743 to K.I., and JP19H05750 to M.I.); Japan Agency for Medical Research and Development (AMED) grant JP18gm5010001 to M.I.; Takeda Science Foundation grants to M.I. The funders had no role in the study design, data collection and analysis, decision to publish, or preparation of the manuscript.

bioRxiv preprint doi: https://doi.org/10.1101/2021.02.12.430913; this version posted February 12, 2021. The copyright holder for this preprint (which was not certified by peer review) is the author/funder, who has granted bioRxiv a license to display the preprint in perpetuity. It is made available under aCC-BY 4.0 International license.

References

1. Matzuk MM, Lamb DJ. The biology of infertility: research advances and clinical challenges. Nat Med. 2008;14(11):1197-213.

2. Mashiko D, Fujihara Y, Satouh Y, Miyata H, Isotani A, Ikawa M. Generation of mutant mice by pronuclear injection of circular plasmid expressing Cas9 and single guided RNA. Sci Rep. 2013;3:3355.

3. Mashiko D, Young SA, Muto M, Kato H, Nozawa K, Ogawa M, et al. Feasibility for a large scale mouse mutagenesis by injecting CRISPR/Cas plasmid into zygotes. Dev Growth Differ. 2014;56(1):122-9.

4. Oji A, Noda T, Fujihara Y, Miyata H, Kim YJ, Muto M, et al. CRISPR/Cas9 mediated genome editing in ES cells and its application for chimeric analysis in mice. Sci Rep. 2016;6:31666.

5. Oura S, Miyata H, Noda T, Shimada K, Matsumura T, Morohoshi A, et al. Chimeric analysis with newly established EGFP/DsRed2-tagged ES cells identify HYDIN as essential for spermiogenesis in mice. Exp Anim. 2019;68(1):25-34.

6. Ikawa M, Inoue N, Benham AM, Okabe M. Fertilization: a sperm's journey to and interaction with the oocyte. J Clin Invest. 2010;120(4):984-94.

7. Lu Y, Oura S, Matsumura T, Oji A, Sakurai N, Fujihara Y, et al. CRISPR/Cas9-mediated genome editing reveals 30 testis-enriched genes dispensable for male fertility in micedagger. Biol Reprod. 2019;101(2):501-11.

8. Miyata H, Castaneda JM, Fujihara Y, Yu Z, Archambeault DR, Isotani A, et al. Genome engineering uncovers 54 evolutionarily conserved and testis-enriched genes that are not required for male fertility in mice. Proc Natl Acad Sci U S A. 2016;113(28):7704-10.

9. Liu Z, Xiang Y, Sun G. The KCTD family of proteins: structure, function, disease relevance. Cell Biosci. 2013;3(1):45.

bioRxiv preprint doi: https://doi.org/10.1101/2021.02.12.430913; this version posted February 12, 2021. The copyright holder for this preprint (which was not certified by peer review) is the author/funder, who has granted bioRxiv a license to display the preprint in perpetuity. It is made available under aCC-BY 4.0 International license.

608 10. Teng X, Aouacheria A, Lionnard L, Metz KA, Soane L, Kamiya A, et al. KCTD: A new gene
609 family involved in neurodevelopmental and neuropsychiatric disorders. CNS Neurosci Ther.
610 2019;25(7):887-902.
611 11. Azizieh R, Orduz D, Van Bogaert P, Bouschet T, Rodriguez W, Schiffmann SN, et al.
612 Progressive myoclonic epilepsy-associated gene KCTD7 is a regulator of potassium conductance in
613 neurons. Mol Neurobiol. 2011;44(1):111-21.
614 12. Usman H, Mathew MK. Potassium channel regulator KCNRG regulates surface
615 expression of Shaker-type potassium channels. Biochem Biophys Res Commun. 2010;391(3):1301-
616 5.
617 13. Kim DM, Chung KS, Choi SJ, Jung YJ, Park SK, Han GH, et al. RhoB induces apoptosis
618 via direct interaction with TNFAIP1 in HeLa cells. Int J Cancer. 2009;125(11):2520-7.
619 14. Nawa M, Kage-Nakadai E, Aiso S, Okamoto K, Mitani S, Matsuoka M. Reduced
620 expression of BTBD10, an Akt activator, leads to motor neuron death. Cell Death Differ.
621 2012;19(8):1398-407.
622 15. De Smaele E, Di Marcotullio L, Moretti M, Pelloni M, Occhione MA, Infante P, et al.
623 Identification and characterization of KCASH2 and KCASH3, 2 novel Cullin3 adaptors
624 suppressing histone deacetylase and Hedgehog activity in medulloblastoma. Neoplasia.
625 2011;13(4):374-85.
626 16. Smaldone G, Pirone L, Balasco N, Di Gaetano S, Pedone EM, Vitagliano L. Cullin 3
627 Recognition Is Not a Universal Property among KCTD Proteins. PLoS One. 2015;10(5):e0126808.
628 17. Canettieri G, Di Marcotullio L, Greco A, Coni S, Antonucci L, Infante P, et al. Histone
629 deacetylase and Cullin3-REN(KCTD11) ubiquitin ligase interplay regulates Hedgehog signalling
630 through Gli acetylation. Nat Cell Biol. 2010;12(2):132-42.
631 18. Choi E, Han C, Park I, Lee B, Jin S, Choi H, et al. A novel germ cell-specific protein,

bioRxiv preprint doi: https://doi.org/10.1101/2021.02.12.430913; this version posted February 12, 2021. The copyright holder for this preprint (which was not certified by peer review) is the author/funder, who has granted bioRxiv a license to display the preprint in perpetuity. It is made available under aCC-BY 4.0 International license.

632 SHIP1, forms a complex with chromatin remodeling activity during spermatogenesis. J Biol Chem.
633 2008;283(50):35283-94.
634 19. Kluin PM, Kramer MF, de Rooij DG. Spermatogenesis in the immature mouse proceeds
635 faster than in the adult. Int J Androl. 1982;5(3):282-94.
636 20. Letunic I, Khedkar S, Bork P. SMART: recent updates, new developments and status in
637 2020. Nucleic Acids Res. 2021;49(D1):D458-D60.
638 21. Larkin MA, Blackshields G, Brown NP, Chenna R, McGettigan PA, McWilliam H, et al.
639 Clustal W and Clustal X version 2.0. Bioinformatics. 2007;23(21):2947-8.
640 22. Endo T, Romer KA, Anderson EL, Baltus AE, de Rooij DG, Page DC. Periodic retinoic
641 acid-STRA8 signaling intersects with periodic germ-cell competencies to regulate spermatogenesis.
642 Proc Natl Acad Sci U S A. 2015;112(18):E2347-56.
643 23. Oakberg EF. A description of spermiogenesis in the mouse and its use in analysis of the
644 cycle of the seminiferous epithelium and germ cell renewal. Am J Anat. 1956;99(3):391-413.
645 24. Hughes SE, Hawley RS. Alternative Synaptonemal Complex Structures: Too Much of a
646 Good Thing? Trends Genet. 2020;36(11):833-44.
647 25. Watanabe D, Okabe M, Hamajima N, Morita T, Nishina Y, Nishimune Y. Characterization
648 of the testis-specific gene 'calmegin' promoter sequence and its activity defined by transgenic
649 mouse experiments. FEBS Lett. 1995;368(3):509-12.
650 26. Kreusch A, Pfaffinger PJ, Stevens CF, Choe S. Crystal structure of the tetramerization
651 domain of the Shaker potassium channel. Nature. 1998;392(6679):945-8.
652 27. Lagger G, O'Carroll D, Rembold M, Khier H, Tischler J, Weitzer G, et al. Essential
653 function of histone deacetylase 1 in proliferation control and CDK inhibitor repression. Embo j.
654 2002;21(11):2672-81.
655 28. Fujihara Y, Kaseda K, Inoue N, Ikawa M, Okabe M. Production of mouse pups from

bioRxiv preprint doi: https://doi.org/10.1101/2021.02.12.430913; this version posted February 12, 2021. The copyright holder for this preprint (which was not certified by peer review) is the author/funder, who has granted bioRxiv a license to display the preprint in perpetuity. It is made available under aCC-BY 4.0 International license.

656 germline transmission-failed knockout chimeras. Transgenic Res. 2013;22(1):195-200.

657 29. Isotani A, Nakanishi T, Kobayashi S, Lee J, Chuma S, Nakatsuji N, et al. Genomic
658 imprinting of XX spermatogonia and XX oocytes recovered from XX<-->XY chimeric testes. Proc
659 Natl Acad Sci U S A. 2005;102(11):4039-44.

660 30. Fang K, Li Q, Wei Y, Zhou C, Guo W, Shen J, et al. Prediction and validation of mouse
661 meiosis-essential genes based on spermatogenesis proteome dynamics. Mol Cell Proteomics. 2020.

662 31. Eaker S, Cobb J, Pyle A, Handel MA. Meiotic prophase abnormalities and metaphase cell
663 death in MLH1-deficient mouse spermatocytes: insights into regulation of spermatogenic progress.
664 Dev Biol. 2002;249(1):85-95.

665 32. McKim KS, Jang JK, Theurkauf WE, Hawley RS. Mechanical basis of meiotic metaphase
666 arrest. Nature. 1993;362(6418):364-6.

667 33. Stogios PJ, Downs GS, Jauhal JJ, Nandra SK, Prive GG. Sequence and structural
668 analysis of BTB domain proteins. Genome Biol. 2005;6(10):R82.

669 34. Huynh KD, Bardwell VJ. The BCL-6 POZ domain and other POZ domains interact with
670 the co-repressors N-CoR and SMRT. Oncogene. 1998;17(19):2473-84.

671 35. Li JY, English MA, Ball HJ, Yeyati PL, Waxman S, Licht JD. Sequence-specific DNA
672 binding and transcriptional regulation by the promyelocytic leukemia zinc finger protein. J Biol
673 Chem. 1997;272(36):22447-55.

674 36. Melnick A, Carlile G, Ahmad KF, Kiang CL, Corcoran C, Bardwell V, et al. Critical
675 residues within the BTB domain of PLZF and Bcl-6 modulate interaction with corepressors. Mol
676 Cell Biol. 2002;22(6):1804-18.

677 37. Ding Z, Gillespie LL, Paterno GD. Human MI-ER1 alpha and beta function as
678 transcriptional repressors by recruitment of histone deacetylase 1 to their conserved ELM2 domain.
679 Mol Cell Biol. 2003;23(1):250-8.

bioRxiv preprint doi: https://doi.org/10.1101/2021.02.12.430913; this version posted February 12, 2021. The copyright holder for this preprint (which was not certified by peer review) is the author/funder, who has granted bioRxiv a license to display the preprint in perpetuity. It is made available under aCC-BY 4.0 International license.

680 38. Itoh T, Fairall L, Muskett FW, Milano CP, Watson PJ, Arnaudo N, et al. Structural and
681 functional characterization of a cell cycle associated HDAC1/2 complex reveals the structural basis
682 for complex assembly and nucleosome targeting. Nucleic Acids Res. 2015;43(4):2033-44.
683 39. Millard CJ, Watson PJ, Celardo I, Gordiyenko Y, Cowley SM, Robinson CV, et al. Class I
684 HDACs share a common mechanism of regulation by inositol phosphates. Mol Cell. 2013;51(1):57-
685 67.
686 40. Dai X, Zhang M, Lu Y, Miao Y, Zhou C, Xiong B. Cullin9 protects mouse eggs from
687 aneuploidy by controlling microtubule dynamics via Survivin. Biochim Biophys Acta.
688 2016;1863(12):2934-41.
689 41. Turnbull RE, Fairall L, Saleh A, Kelsall E, Morris KL, Ragan TJ, et al. The MiDAC
690 histone deacetylase complex is essential for embryonic development and has a unique multivalent
691 structure. Nat Commun. 2020;11(1):3252.
692 42. Noda T, Sakurai N, Nozawa K, Kobayashi S, Devlin DJ, Matzuk MM, et al. Nine genes
693 abundantly expressed in the epididymis are not essential for male fecundity in mice. Andrology.
694 2019;7(5):644-53.
695 43. Oura S, Kazi S, Savolainen A, Nozawa K, Castaneda J, Yu Z, et al. Cfap97d1 is important
696 for flagellar axoneme maintenance and male mouse fertility. PLoS Genet. 2020;16(8):e1008954.
697 44. Kishiro Y, Kagawa M, Naito I, Sado Y. A novel method of preparing rat-monoclonal
698 antibody-producing hybridomas by using rat medial iliac lymph node cells. Cell Struct Funct.
699 1995;20(2):151-6.
700 45. Sado Y, Inoue S, Tomono Y, Omori H. Lymphocytes from enlarged iliac lymph nodes as
701 fusion partners for the production of monoclonal antibodies after a single tail base immunization
702 attempt. Acta Histochem Cytochem. 2006;39(3):89-94.
703 46. Oji A, Isotani A, Fujihara Y, Castaneda JM, Oura S, Ikawa M. Tesmin, Metallothionein-

bioRxiv preprint doi: https://doi.org/10.1101/2021.02.12.430913; this version posted February 12, 2021. The copyright holder for this preprint (which was not certified by peer review) is the author/funder, who has granted bioRxiv a license to display the preprint in perpetuity. It is made available under aCC-BY 4.0 International license.

704 Like 5, is Required for Spermatogenesis in Micedagger. Biol Reprod. 2020;102(4):975-83.

705 47. Wellard SR, Hopkins J, Jordan PW. A Seminiferous Tubule Squash Technique for the

706 Cytological Analysis of Spermatogenesis Using the Mouse Model. J Vis Exp. 2018(132).

707

708

bioRxiv preprint doi: https://doi.org/10.1101/2021.02.12.430913; this version posted February 12, 2021. The copyright holder for this preprint (which was not certified by peer review) is the author/funder, who has granted bioRxiv a license to display the preprint in perpetuity. It is made available under aCC-BY 4.0 International license.

Figure legends

Fig 1. Production of *Kctd19*$^{del/del}$ mice and fertility analysis.

(A) RT-PCR using multi-tissue cDNA. *Actb* was used as a loading control. (B) RT-PCR using postnatal testis cDNA. *Actb* was used as a loading control. (C) Schematic of KCTD19 protein structure and antigen position. (D) Phylogenetic tree constructed by ClustalW with KCTD19 sequences of various mammals. (E) Gene map of *Kctd19*. Black and white boxes indicate coding and non-coding regions, respectively. Black arrows and arrowheads indicate primers for genotyping and gRNAs for genome editing, respectively. (F) An example of genotyping PCR with two primer sets shown in E. (G) DNA sequencing for deletion verification. (H) Immunoblotting with antibodies against mouse KCTD19. Red arrows indicate the expected molecular size of KCTD19. GAPDH was used as a loading control. (I) The result of mating tests. Pups/plug: 8.8±2.4 [WT]; 0 [*del/del*] (J) Pup numbers obtained from mating pairs of *Kctd19*$^{del/del}$ females *and Kctd19*$^{wt/del}$ males (7.8±2.2).

Fig 2. Histological analysis of *Kctd19*$^{del/del}$ mice.

(A) Testis morphology and (B) testis/body weight of *Kctd19*$^{wt/del}$ and *Kctd19*$^{del/del}$ adult mice at 12 weeks. Testis/body weight: 4.5±0.2 x 10^{-3} [*wt/del*], 1.2±0.3 x 10^{-3} [*del/del*]. Error bars indicate one standard deviation. (C) PAS staining of seminiferous tubules of adult mice. The seminiferous epithelium cycle was determined by germ cell position and nuclear morphology. (D) TUNEL staining of seminiferous tubules of adult mice counterstained with hematoxylin. (E) PAS staining of cauda epididymis of adult mice. (F & G) Immunostaining of seminiferous tubules of adult mice. The seminiferous epithelium cycle was determined by cell position, nuclear morphology, and morphology of acrosome staining with AlexaFlour 568-conjugated lectin PNA.

bioRxiv preprint doi: https://doi.org/10.1101/2021.02.12.430913; this version posted February 12, 2021. The copyright holder for this preprint (which was not certified by peer review) is the author/funder, who has granted bioRxiv a license to display the preprint in perpetuity. It is made available under aCC-BY 4.0 International license.

Fig 3. Cytological analysis of *Kctd19*$^{del/del}$ spermatocytes.

(A & B) Immunostaining of spread nuclei from prophase spermatocytes collected from adult (A) and juvenile (B) mice. (C) The percentage of each meiotic prophase stage present is determined by immunostained spread nuclei samples. (D) Giemsa staining of spread nuclei of metaphase I spermatocytes. (E) Immunostaining of prophase spermatocytes with antibodies against CENPC and α-TUBULIN. Right panels (1 – 4) show additional *Kctd19*$^{del/del}$ spermatocytes. Red arrows indicate misaligned chromosomes. (F) The percentage of metaphase I spermatocytes with misaligned chromosomes. (G) Immunostaining of prophase spermatocytes with antibodies against SYCP3 and αTUBULIN. Right panels (1 – 4) show additional *Kctd19*$^{del/del}$ spermatocytes. Red and yellow arrows indicate misaligned chromosomes and SYCP3 polycomplexes, respectively. (H) The percentage of metaphase I spermatocytes with SYCP3 polycomplexes.

Fig 4. Transgenic (Tg) rescue of *Kctd19*$^{del/del}$ mice.

(A) Schematic of Tg mouse production. Red and yellow boxes indicate affinity tags and *Kctd19* ORF, respectively. Black arrows indicate primers for genotyping. (B) An example of PRC genotyping with two primer sets shown in A. (C & D) Immunoblotting with antibodies against FLAG (C) and HA (D) for determining expression levels. (E & F) Immunoprecipitation with antibodies against FLAG (E) and HA (F) and immunoblotting with antibodies against HA and FLAG, respectively. (G) Schematics of fertility determination of Tg mice. (H & I) Two-cell embryos obtained from WT females mated with *Kctd19*$^{del/del}$ males with transgenes. (J) Testis morphology and (K) testis/body weight of WT and *Kctd19*$^{del/del}$, Tg #1 adult mice at 8 weeks. Testis/body weight: 3.2 ± 0.1 [WT]; 4.7 ± 1.6 [*Kctd19*$^{del/del}$, Tg #1]. Error bars indicate one

bioRxiv preprint doi: https://doi.org/10.1101/2021.02.12.430913; this version posted February 12, 2021. The copyright holder for this preprint (which was not certified by peer review) is the author/funder, who has granted bioRxiv a license to display the preprint in perpetuity. It is made available under aCC-BY 4.0 International license.

757 standard deviation. (L) PAS staining of seminiferous tubules of adult mice. The seminiferous
758 epithelium cycle was determined by germ cell position and nuclear morphology. (M)
759 Immunostaining of seminiferous tubules of adult mice. The seminiferous epithelium cycle was
760 determined by cell position, nuclear morphology, and morphology of the acrosome stained
761 with AlexaFlour 568-conjugated lectin PNA.
762
763 **Fig 5. IP-MS analysis with anti-KCTD19 antibody**
764 (A & B) Silver staining of IP eluting samples with rabbit pAb (A) and rat mAb #1 (B). Two
765 juvenile WT mice and two adult *Kctd19*$^{del/del}$ mice were used for each experiment. (C) The list
766 of identified proteins by MS analysis. The quantitative value was calculated using Scaffold
767 software (D) Immunoprecipitation with an anti-HDAC1 antibody and immunoblotting with an
768 anti-HDAC1 antibody. For input sample, 50 μg of testis lysate was used. (E) Immunoblotting
769 with an anti-HDAC1 antibody. GPADH was used as a loading control. (F) Immunostaining with
770 an anti-HDAC1 antibody. The seminiferous epithelium cycle was determined by cell position,
771 nuclear morphology, and morphology of the acrosome stained with AlexaFlour 568-conjugated
772 lectin PNA.
773
774 **Fig 6. Chimeric analysis of *Zfp541* KO spermatocytes**
775 (A) RT-PCR using multi-tissue cDNA. *Actb* was used as a loading control. (B) RT-PCR using
776 postnatal testis cDNA. *Actb* was used as a loading control. (C) Gene map of *Zfp541*. Black
777 and white boxes indicate coding and non-coding regions, respectively. Black arrows and
778 arrowheads indicate primers for genotyping and gRNAs for genome editing, respectively. (D)
779 Genotyping PCR with two primer sets in C for ES cell clones used in this study. (E) Schematics
780 of chimeric mice production. ESC-derived cells were labeled with GFP fluorescence. (F) PAS

bioRxiv preprint doi: https://doi.org/10.1101/2021.02.12.430913; this version posted February 12, 2021. The copyright holder for this preprint (which was not certified by peer review) is the author/funder, who has granted bioRxiv a license to display the preprint in perpetuity. It is made available under aCC-BY 4.0 International license.

781 staining of seminiferous tubules of chimeric mice. ES cell-derived *Zfp541*-KO spermatocytes
782 were identified by immunohistochemistry against GFP. (G) TUNEL staining of seminiferous
783 tubules of chimeric mice counterstained with hematoxylin. ES cell-derived *Zfp541*-KO
784 spermatocytes were identified by immunohistochemistry against GFP. (H & I) Immunostaining
785 of seminiferous tubules of chimeric mice with antibodies against KCTD19 (H) and HDAC1 (I).
786 ES cell-derived *Zfp541*-KO spermatocytes were identified by GFP immunostaining. (J)
787 Immunostaining of spread nuclei of prophase spermatocytes collected from XY->XX chimeric
788 mice. Red and yellow boxes were magnified in the right panels. (K) The percentage of cells in
789 various meiotic prophase stages counted with immunostained spread nuclei samples.
790
791

bioRxiv preprint doi: https://doi.org/10.1101/2021.02.12.430913; this version posted February 12, 2021. The copyright holder for this preprint (which was not certified by peer review) is the author/funder, who has granted bioRxiv a license to display the preprint in perpetuity. It is made available under aCC-BY 4.0 International license.

Supporting information

Fig S1. Sequence comparison of KCTD19 in various mammals.

Prortein sequence comparison of KCTD19 in cattle (NP_001098862.1), pig (XP_003126977.2), dog (XP_022275030.1), fox (XP_025867456.1), cat (XP_023101865.1), bat (XP_027998908.1), human (NP_001094385.1), chimpanzee (XP_523391.2), rhesus monkey (XP_014981866.1), mouse (NP_808459.1), rat (NP_001292128.1), and golden hamster (XP_021086458.1).

Fig S2. Production of *Kctd19*-ΔPOZ mice and fertility analysis.

(A) Gene map of *Kctd19*. Black and white boxes indicate coding and non-coding regions, respectively. Black arrows and arrowheads indicate primers for genotyping and gRNAs for genome editing, respectively. (B) An example of genotyping PCR with two primer sets shown in S2A. (C) DNA sequencing verify the deletion. (D) RT-PCR using tetis cDNA obtained from WT and *ΔPOZ/ΔPOZ* mice. *Actb* was used as a loading control. (E) Immunoblotting using tetis lysates obtained from WT, *del/del*, and *ΔPOZ/ΔPOZ* mice. (F) PAS staining of seminiferous tubules of adult mice. The seminiferous epithelium cycle was determined by germ cell position and nuclear morophology.

Fig S3. Sequence comparison of ZFP541 in various mammals.

Prortein sequence comparison of ZFP541 or ZNF541 proteins from various mammals: cattle (XP_015313711.2), pig (XP_020950303.1), dog (XP_005616437.1), fox (XP_025869832.1), cat (XP_023100994.1), bat (XP_008152641.1), human (NP_001264004.1), chimpanzee (XP_016791837.1), rhesus monkey (XP_014979842.2), mouse (NP_001092747.1), rat (NP_001100928.2), and golden hamster (XP_021078928.1).

bioRxiv preprint doi: https://doi.org/10.1101/2021.02.12.430913; this version posted February 12, 2021. The copyright holder for this preprint (which was not certified by peer review) is the author/funder, who has granted bioRxiv a license to display the preprint in perpetuity. It is made available under aCC-BY 4.0 International license.

816

817 **Fig S4. Production of XY->XX chimeric mice and their feature.**

818 (A) Schematic of XY->XX chimeric mice production. XX prospermatogonia are eliminated

819 around PND2. (B) Testis section from chimeric mice. ES cell-derived cells were labeled with

820 GFP fluorescence. Astarisk indicates depleted tubules.

Figure1

bioRxiv preprint doi: https://doi.org/10.1101/2021.02.12.430913; this version posted February 12, 2021. The copyright holder for this preprint (which was not certified by peer review) is the author/funder, who has granted bioRxiv a license to display the preprint in perpetuity. It is made available under aCC-BY 4.0 International license.

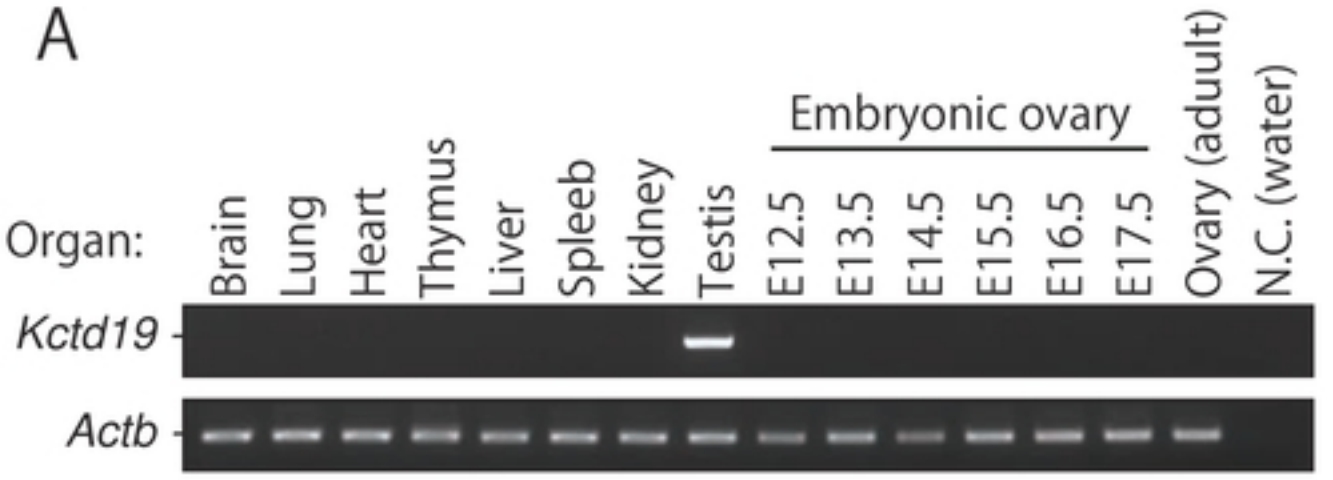

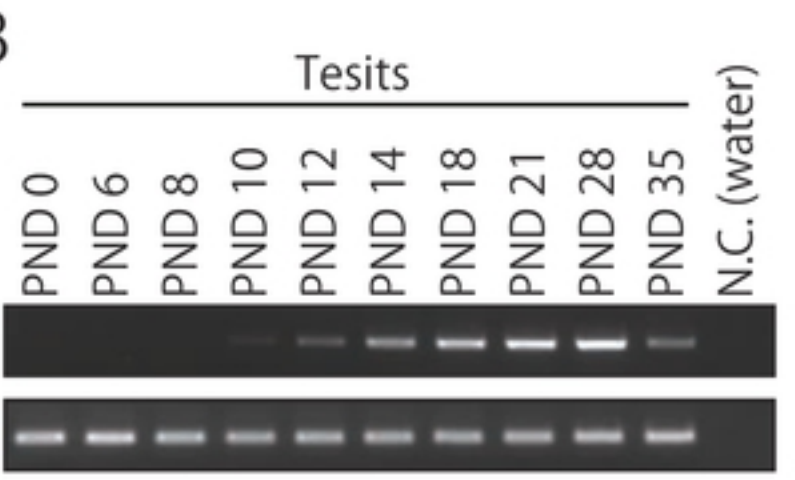

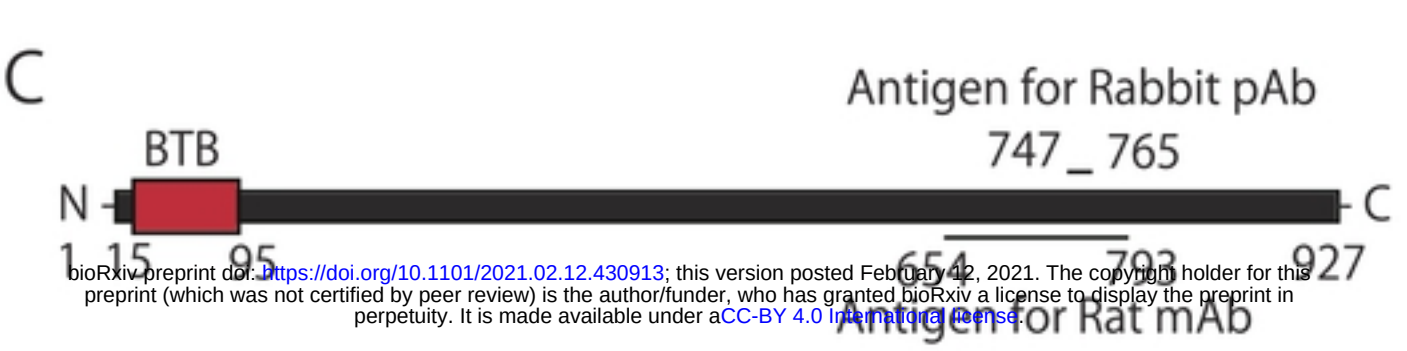

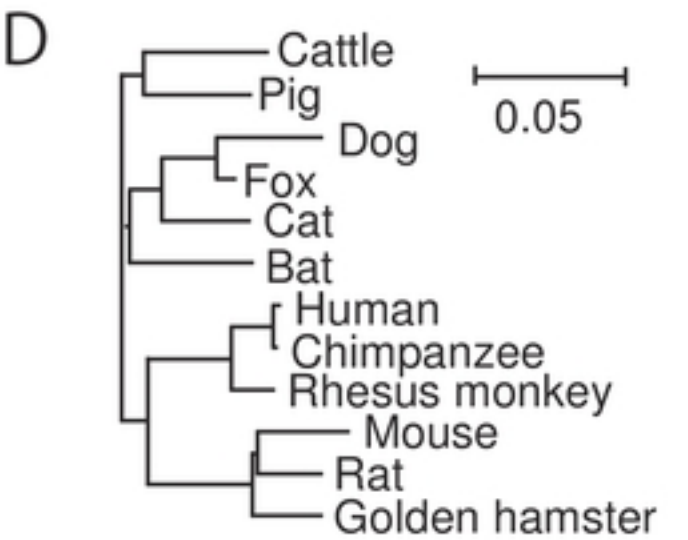

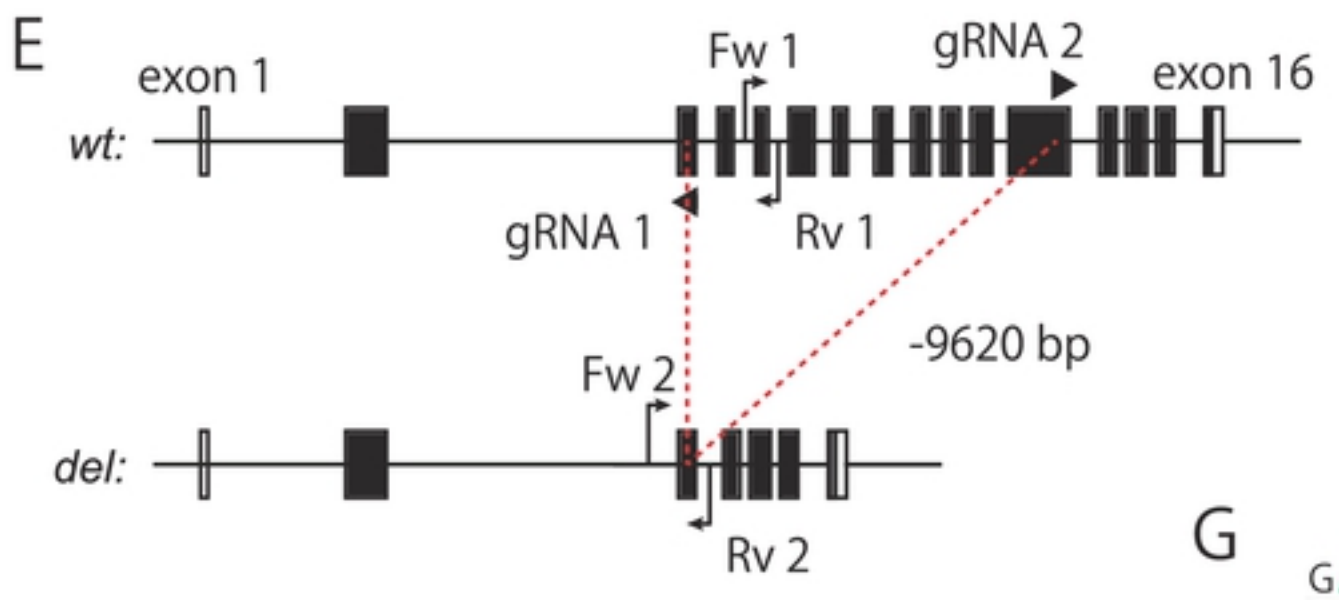

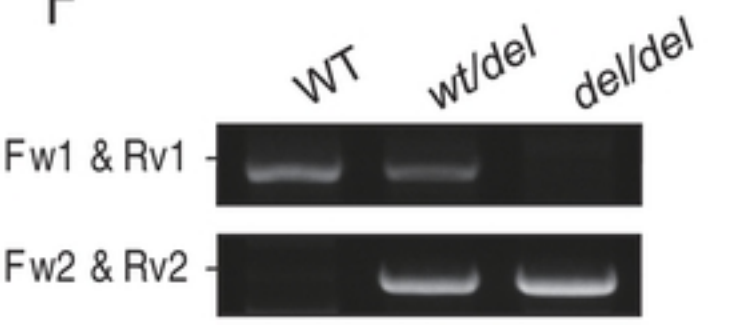

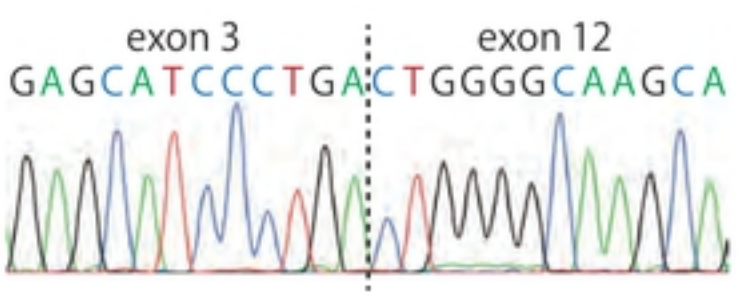

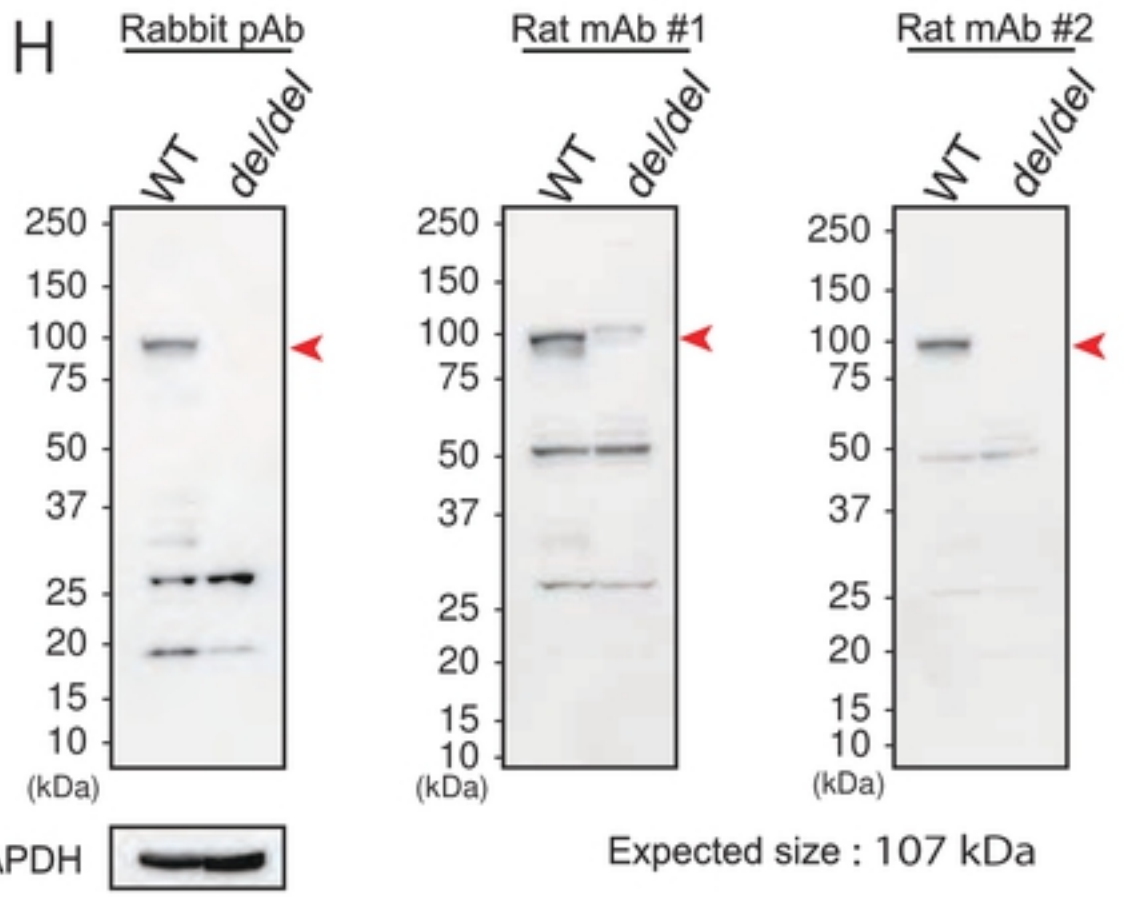

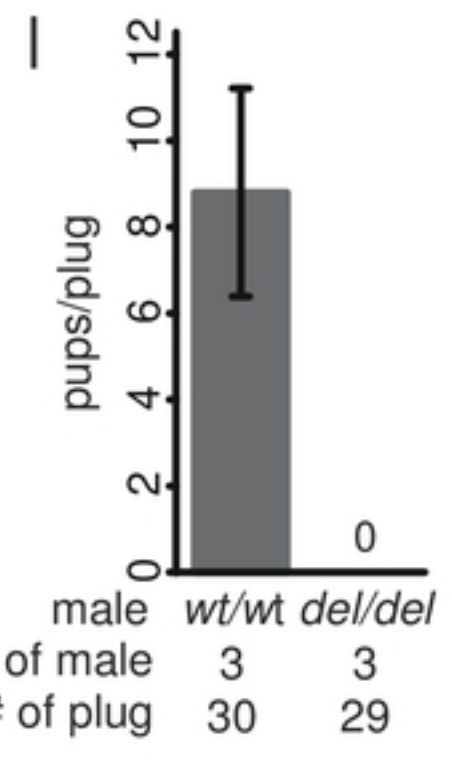

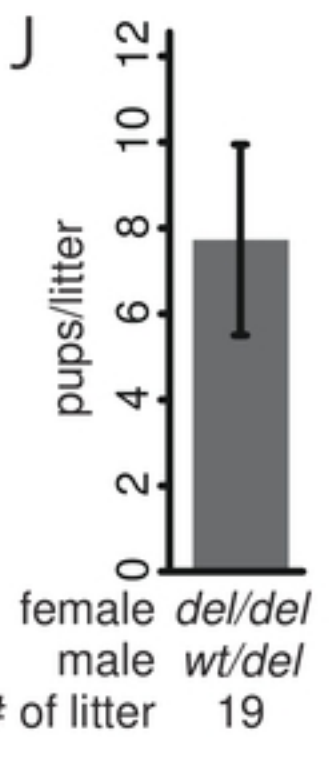

Figure2

bioRxiv preprint doi: https://doi.org/10.1101/2021.02.12.430913; this version posted February 12, 2021. The copyright holder for this preprint (which was not certified by peer review) is the author/funder, who has granted bioRxiv a license to display the preprint in perpetuity. It is made available under aCC-BY 4.0 International license.

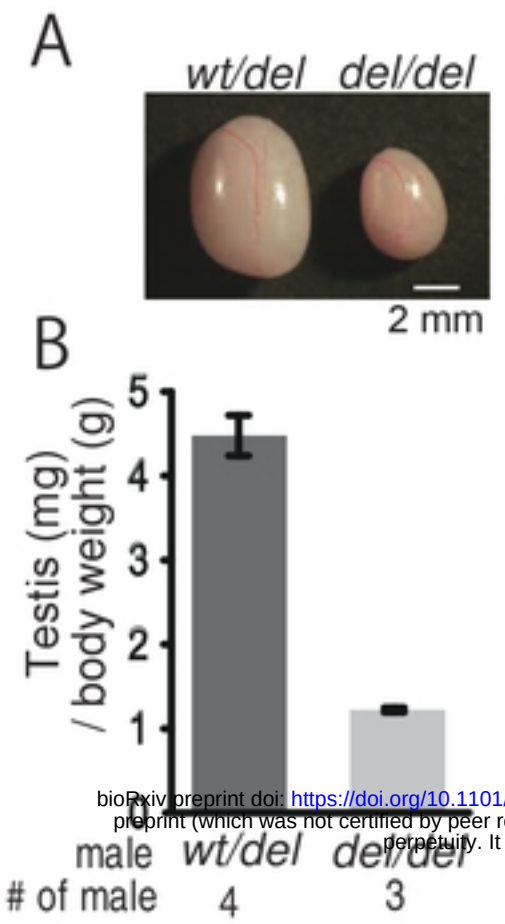

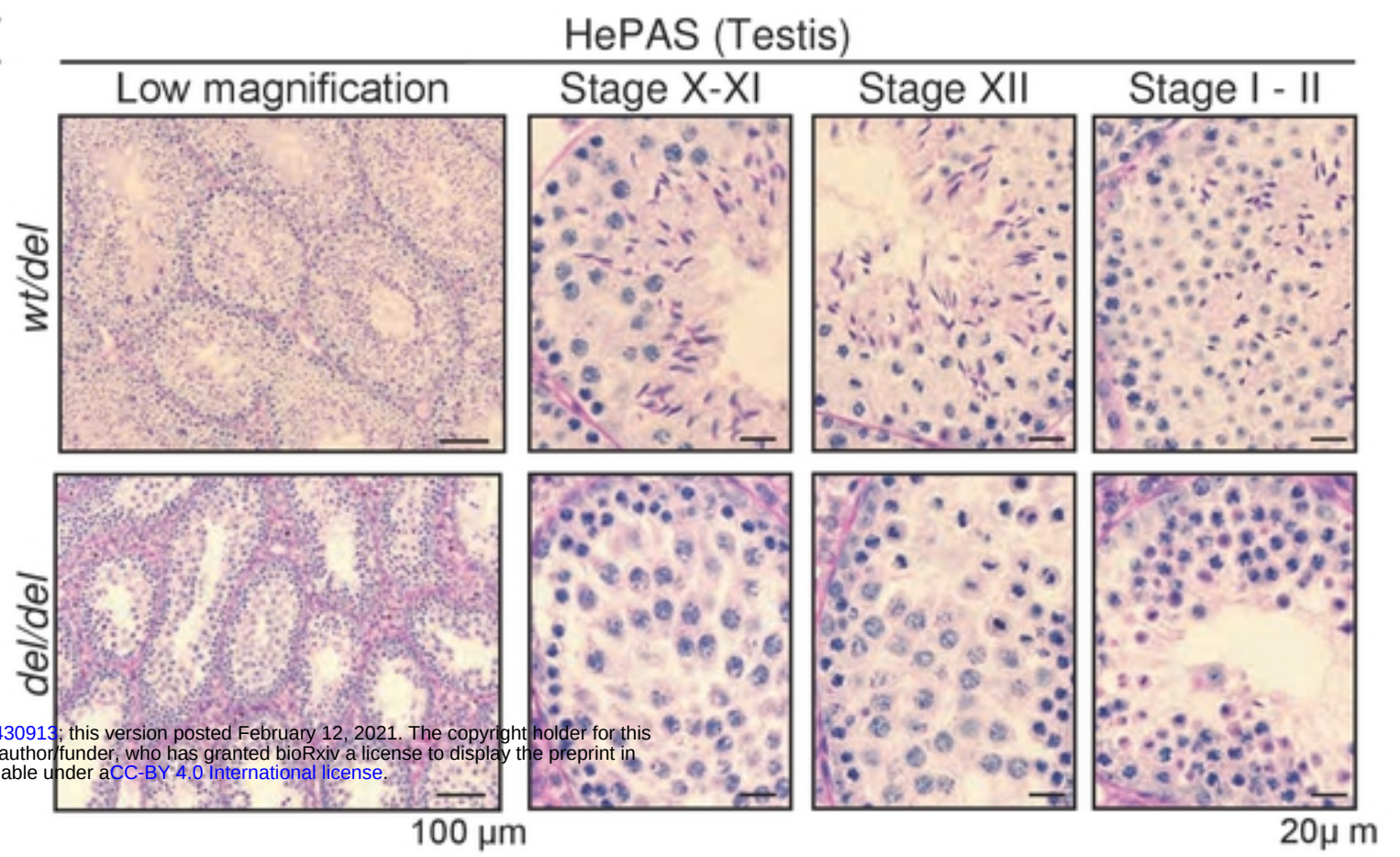

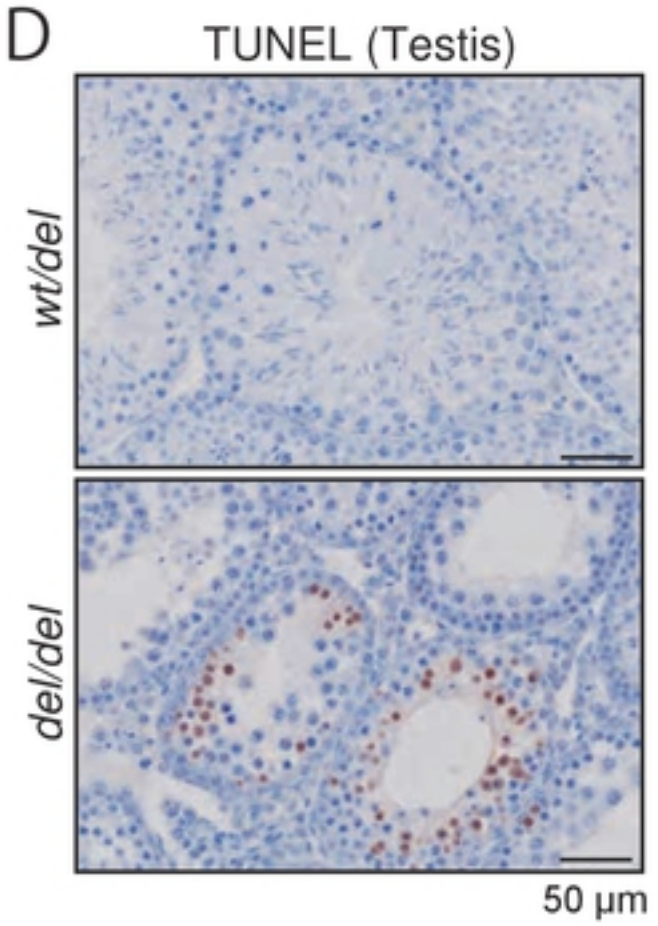

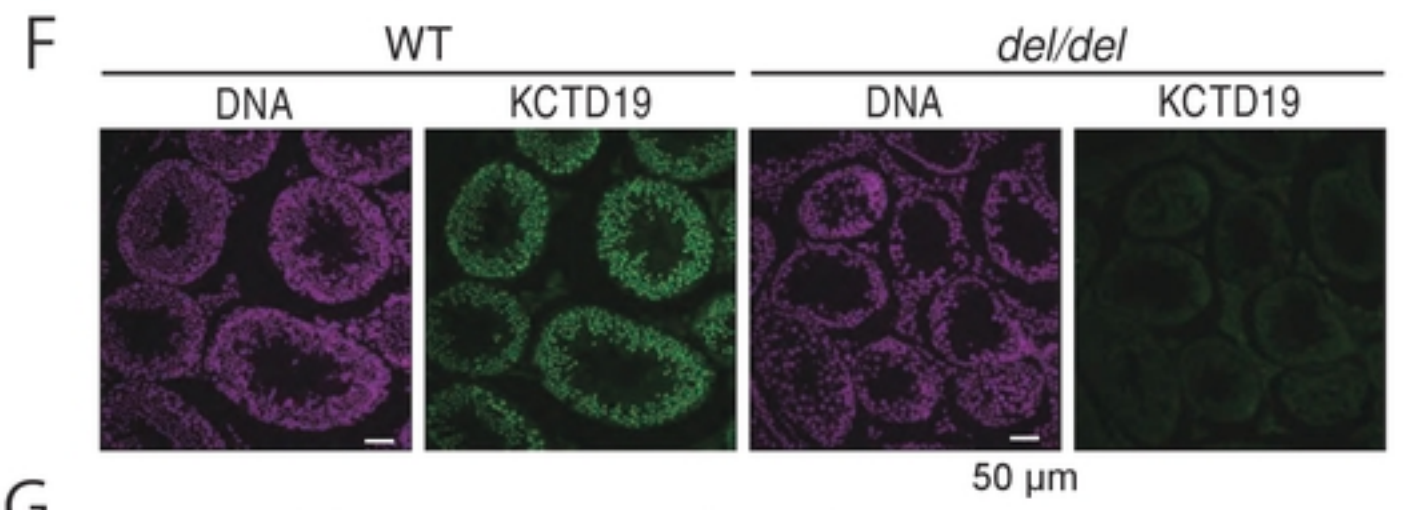

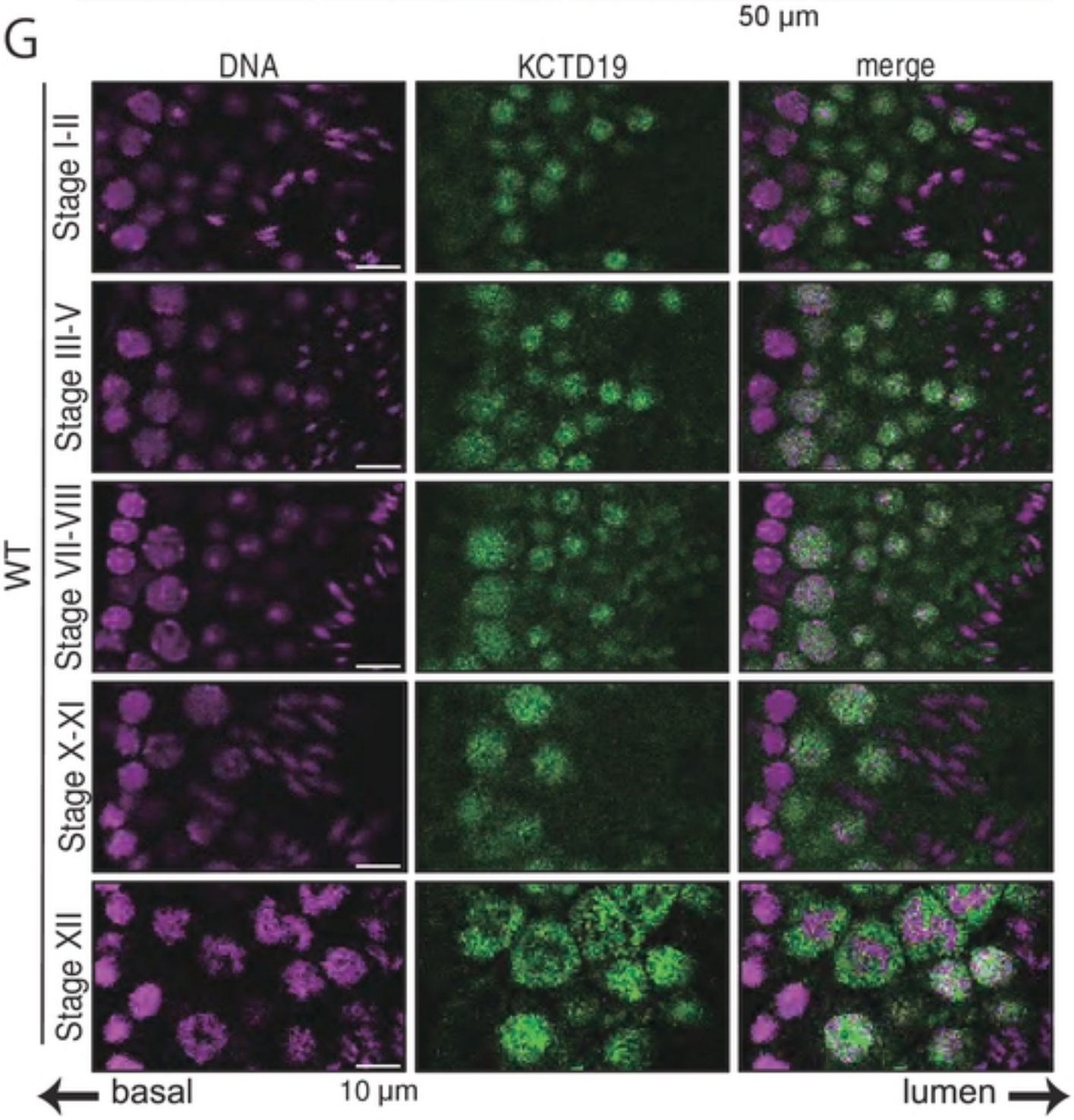

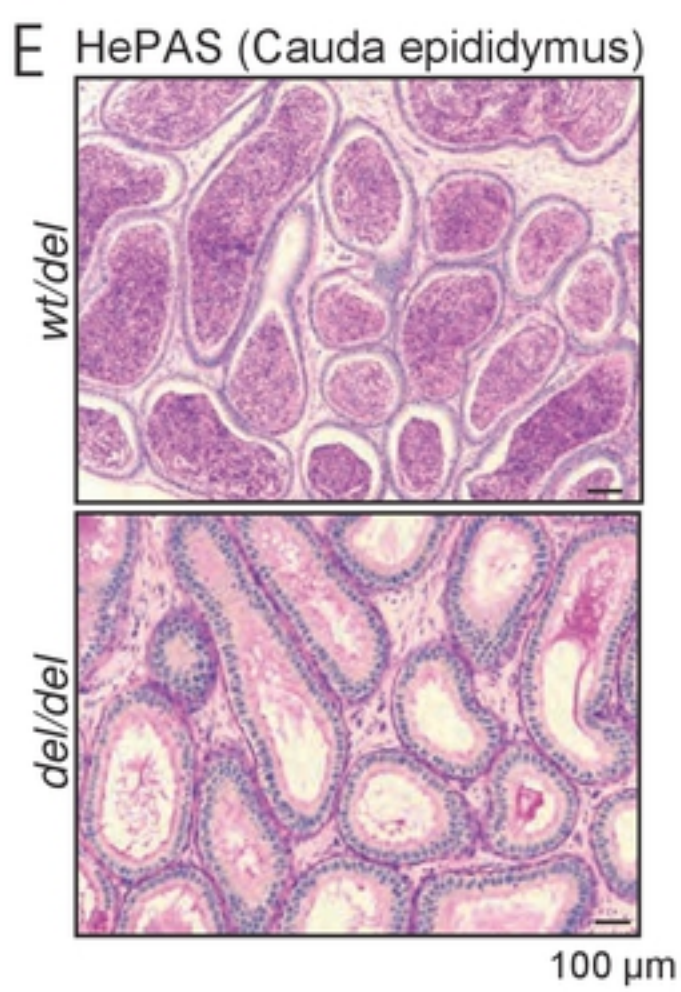

Figure3

bioRxiv preprint doi: https://doi.org/10.1101/2021.02.12.430913; this version posted February 12, 2021. The copyright holder for this preprint (which was not certified by peer review) is the author/funder, who has granted bioRxiv a license to display the preprint in perpetuity. It is made available under aCC-BY 4.0 International license.

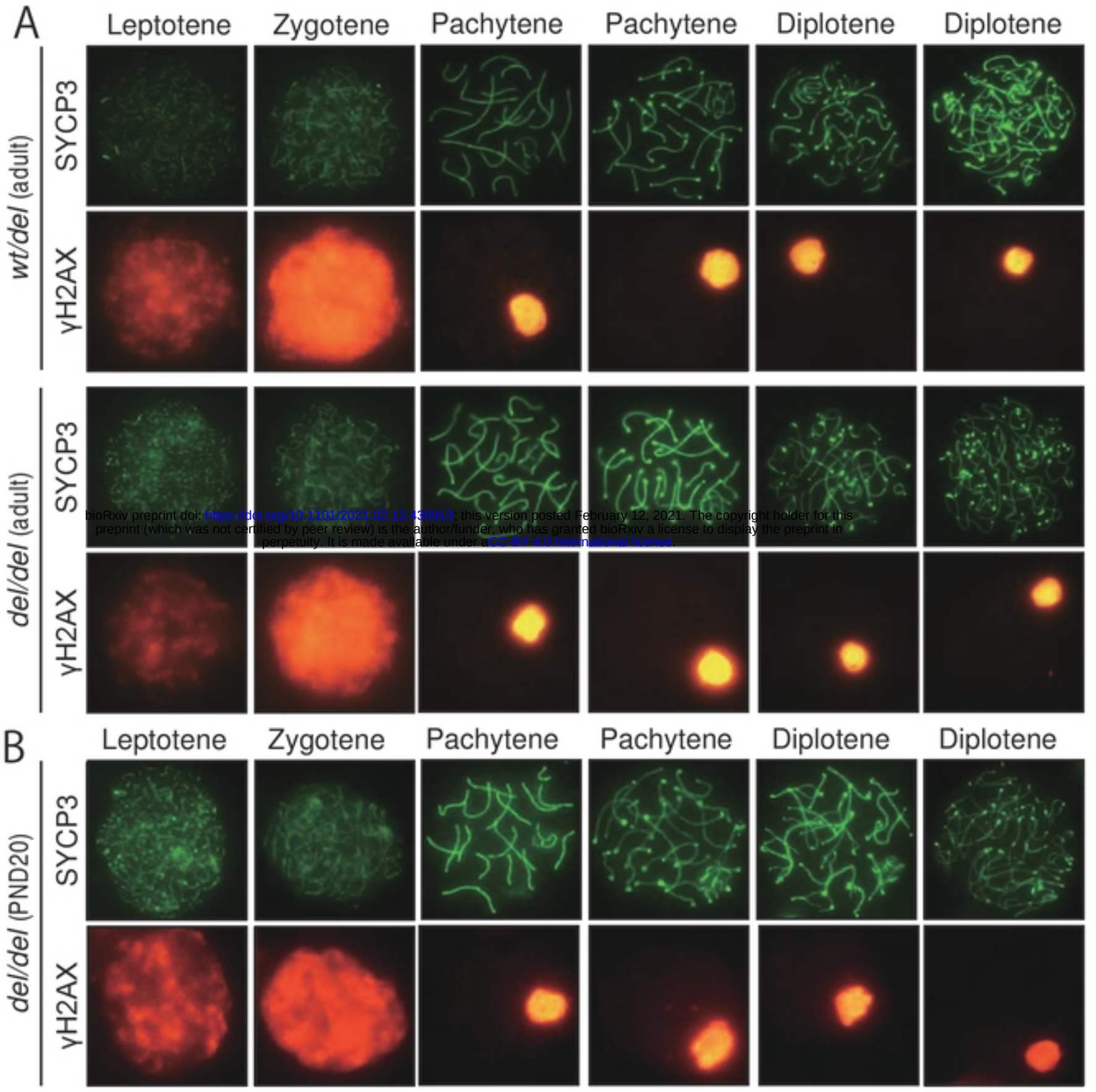

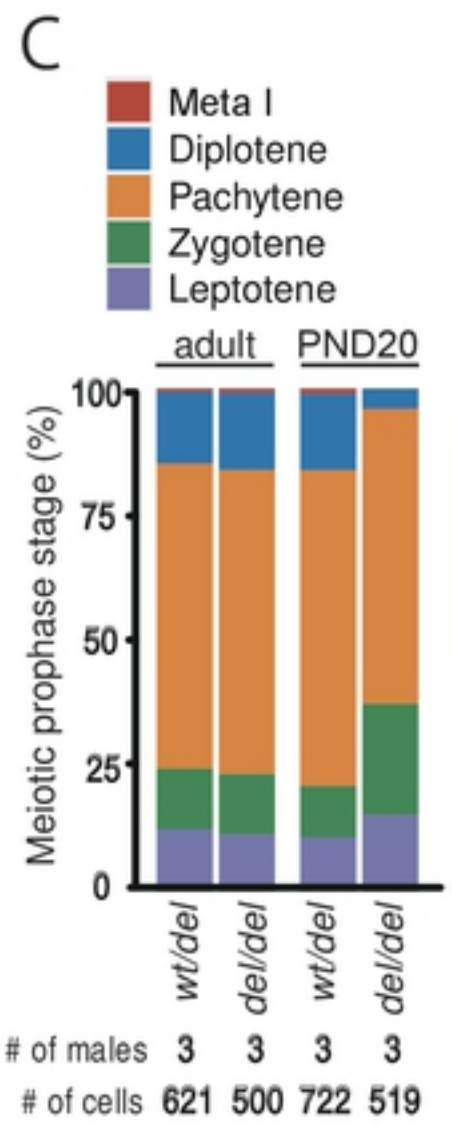

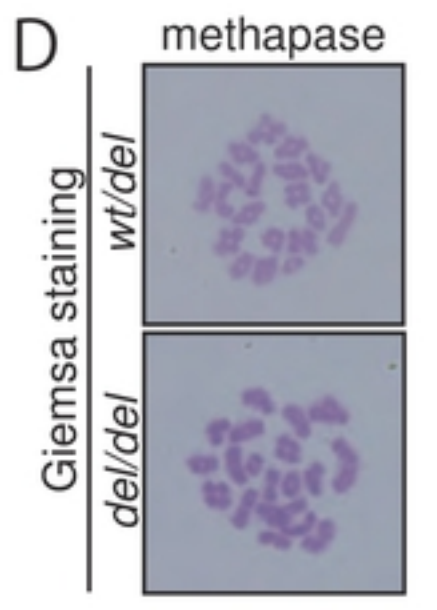

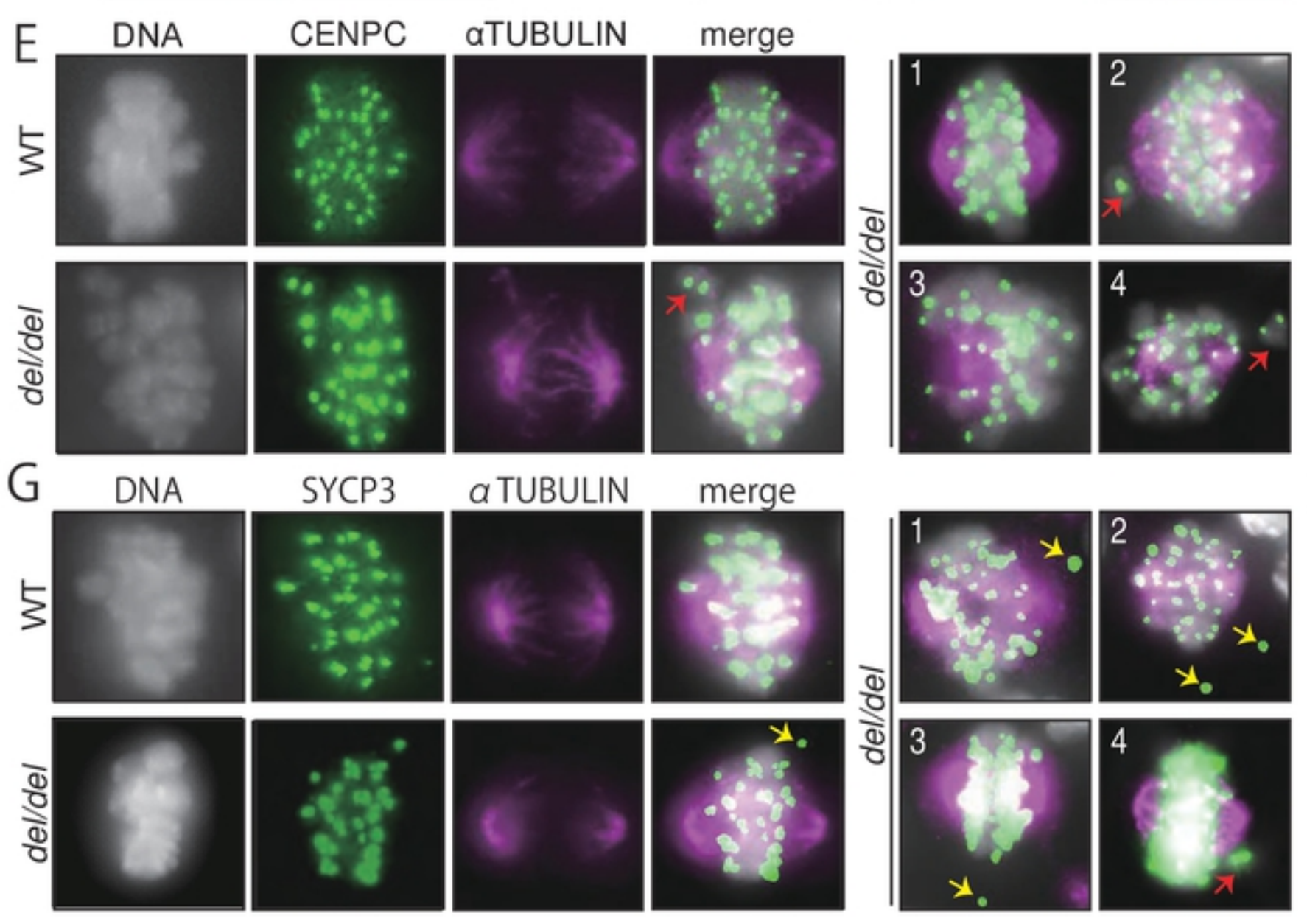

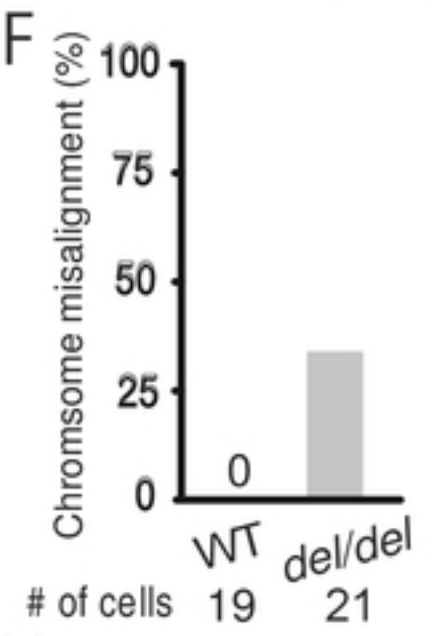

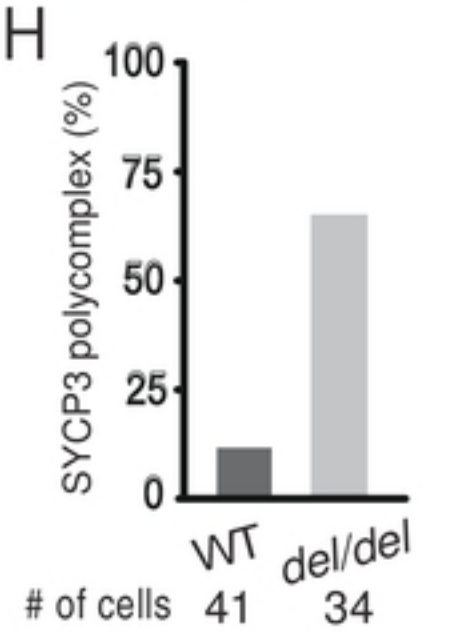

Figure4

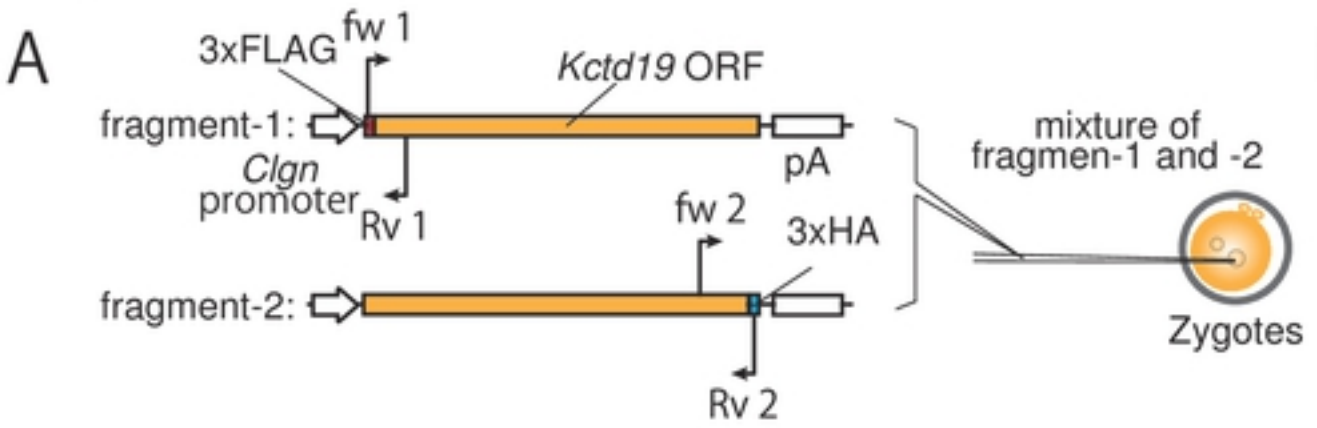

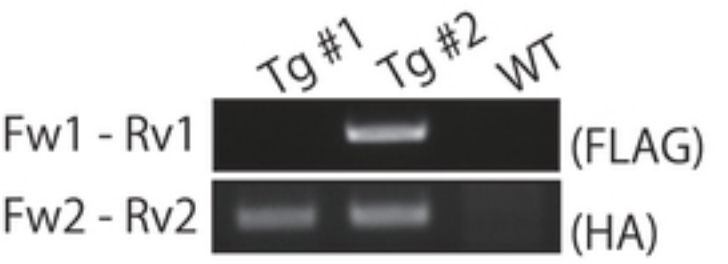

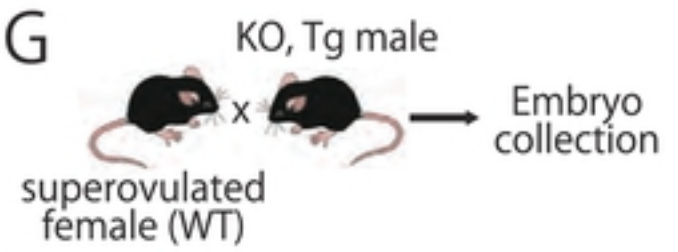

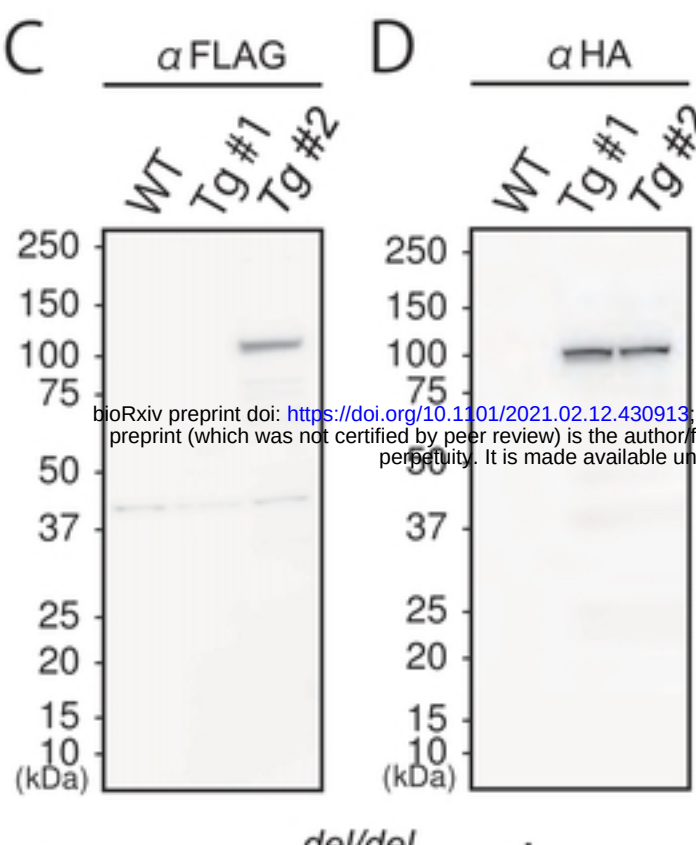

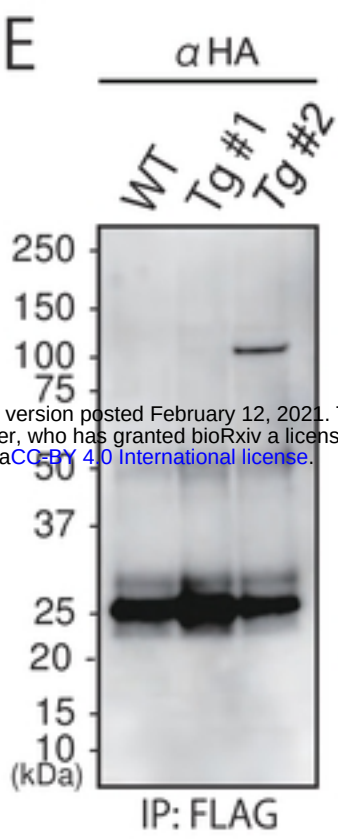

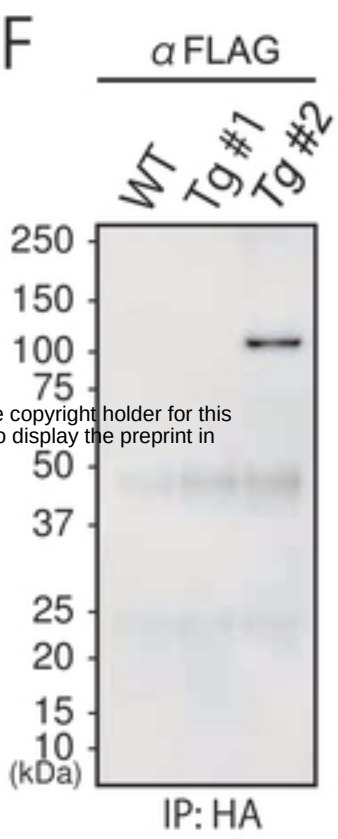

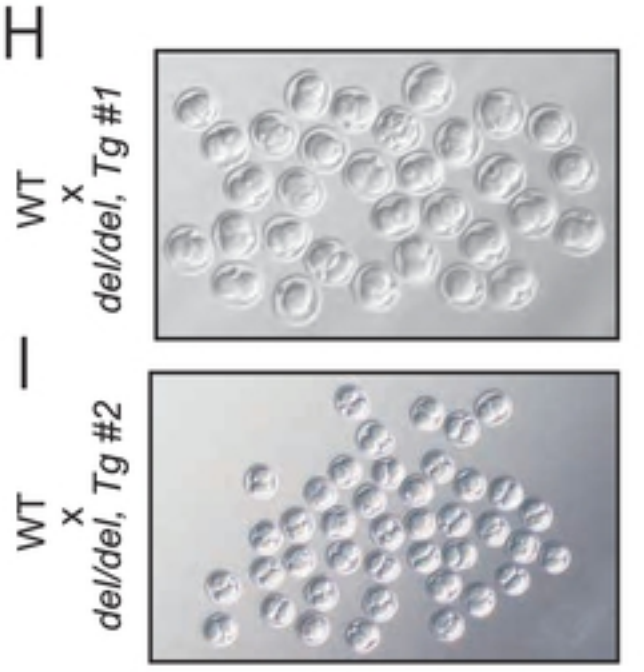

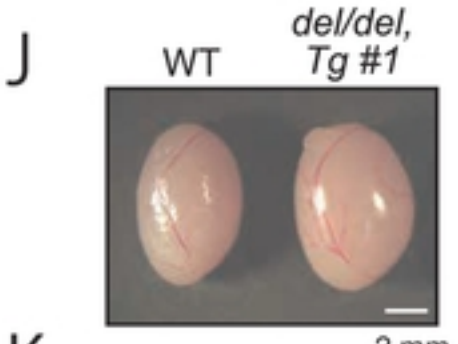

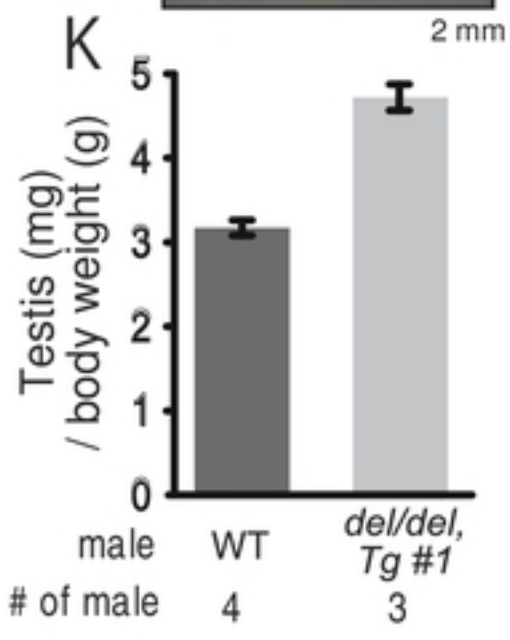

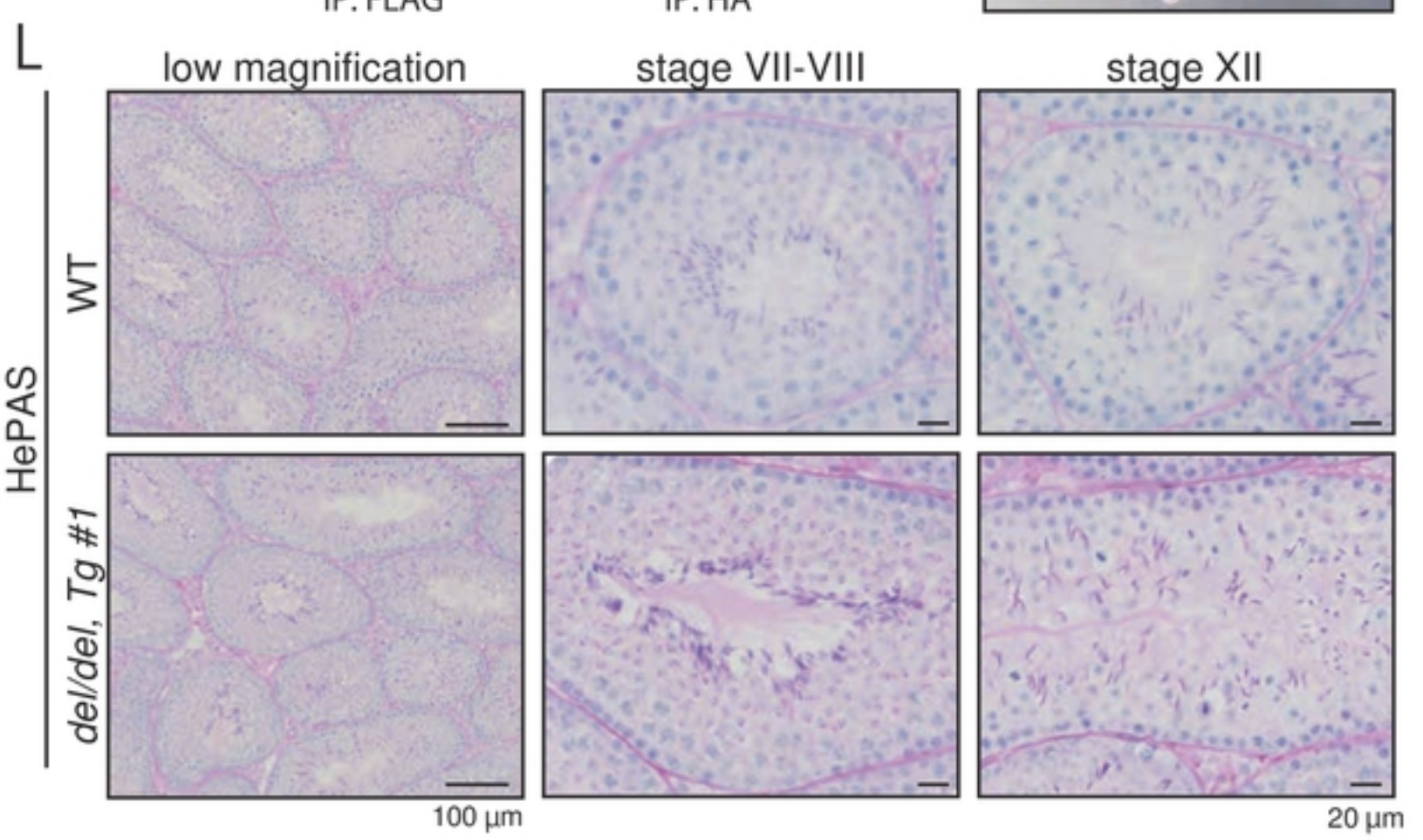

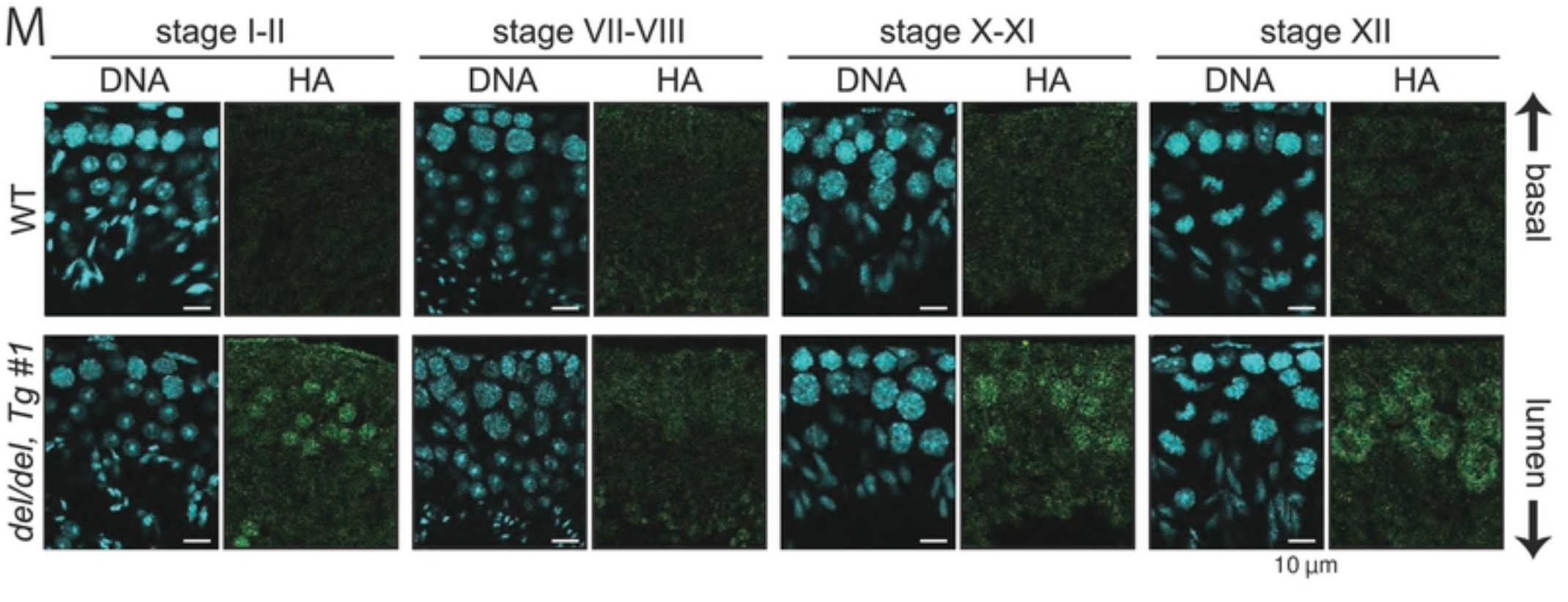

bioRxiv preprint doi: https://doi.org/10.1101/2021.02.12.430913; this version posted February 12, 2021. The copyright holder for this preprint (which was not certified by peer review) is the author/funder, who has granted bioRxiv a license to display the preprint in perpetuity. It is made available under aCC-BY 4.0 International license.

Figure5

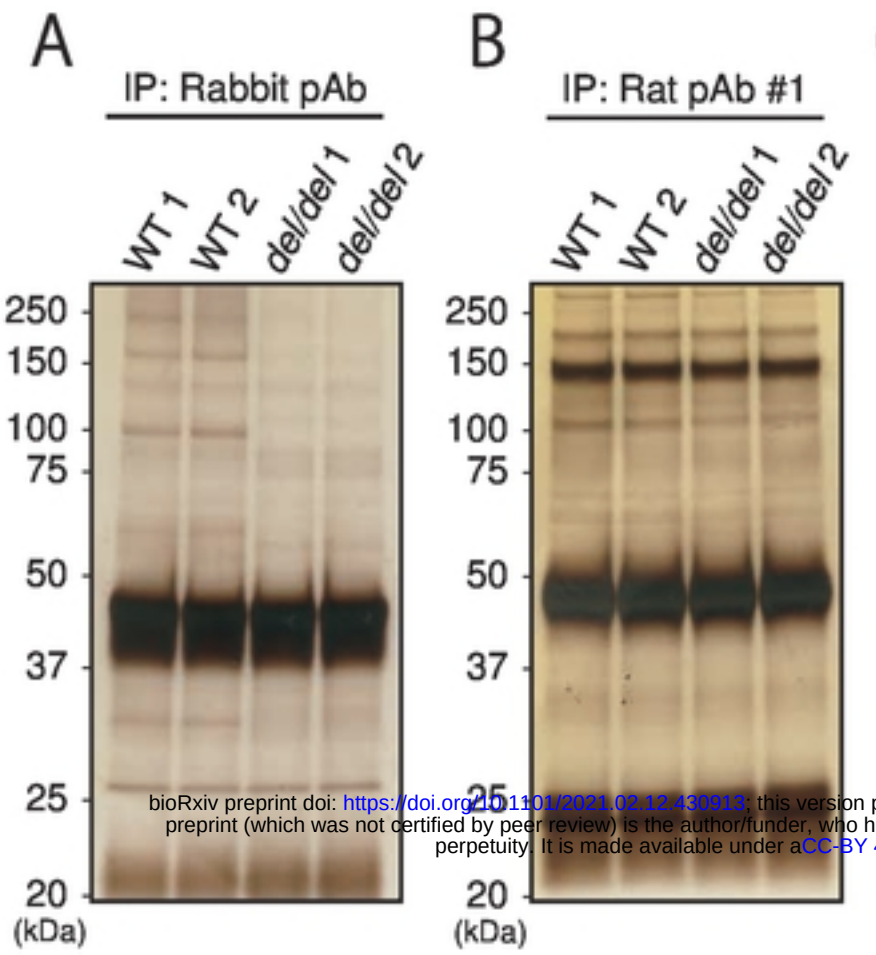

C

Protein	MW	Accession Number	Quantitative Value (Normalized Total Spectra)							
			WT (PND21)				*del/del*			
			Rabbit pAb		Rat mAb #1		Rabbit pAb		Rat mAb #1	
			(N=1)	(N=2)	(N=1)	(N=2)	(N=1)	(N=2)	(N=1)	(N=2)
ZNF541	148 kDa	Q0GGX2	77.186	106.28	22.173	13.632	0	0	0	0
KCTD19	105 kDa	Q562E2	70.169	73.759	33.742	24.858	0	0	0	0
CUL9	209 kDa	Q80TT8	14.911	26.966	0	0	0	0	0	0
HDAC1	55 kDa	O09106	11.403	15.069	2.8921	4.0093	0	0	0	0
ACBD5	57 kDa	Q5XG73	7.8941	11.103	0	0	0	0	0	0
DNTTIP1	37 kDa	Q99LB0	7.0169	8.7241	0	0	0	0	0	0
HSPA1L	71 kDa	P16627	0	0	0	14.434	0	0	0	0
IMMT	84 kDa	Q8CAQ8	4.3856	7.931	0	0	0	0	0	0
PEX5	71 kDa	O09012	6.1398	5.5517	0	0	0	0	0	0
DNAJA1	45 kDa	P63037	2.6314	2.3793	0	0	0	0	0	0
ATP2A2	115 kDa	O55143	2.6314	2.3793	0	0	0	0	0	0
[illegible]	[illegible]	[illegible]	2.6314	2.3793	0	0	0	0	0	0
VAPA	28 kDa	Q9WV55	1.7542	3.1724	0	0	0	0	0	0
SATL1	83 kDa	Q9D5N8	0	0	0	4.8112	0	0	0	0
MAVS	53 kDa	Q8VCF0	2.6314	1.5862	0	0	0	0	0	0
RPL18	22 kDa	P35980	2.6314	1.5862	0	0	0	0	0	0
DDX5	69 kDa	Q61656	1.7542	2.3793	0	0	0	0	0	0
SETX	298 kDa	A2AKX3	1.7542	1.5862	0	0	0	0	0	0
PCBP1	37 kDa	P60335	1.7542	1.5862	0	0	0	0	0	0
RPL3	46 kDa	P27659	1.7542	1.5862	0	0	0	0	0	0

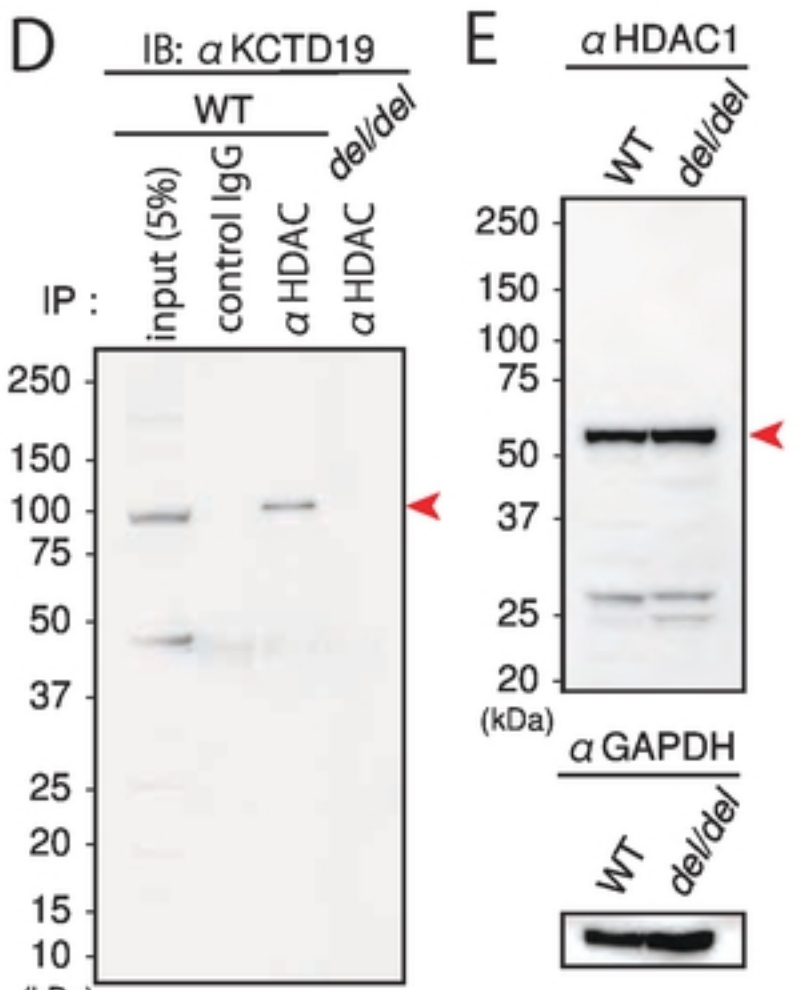

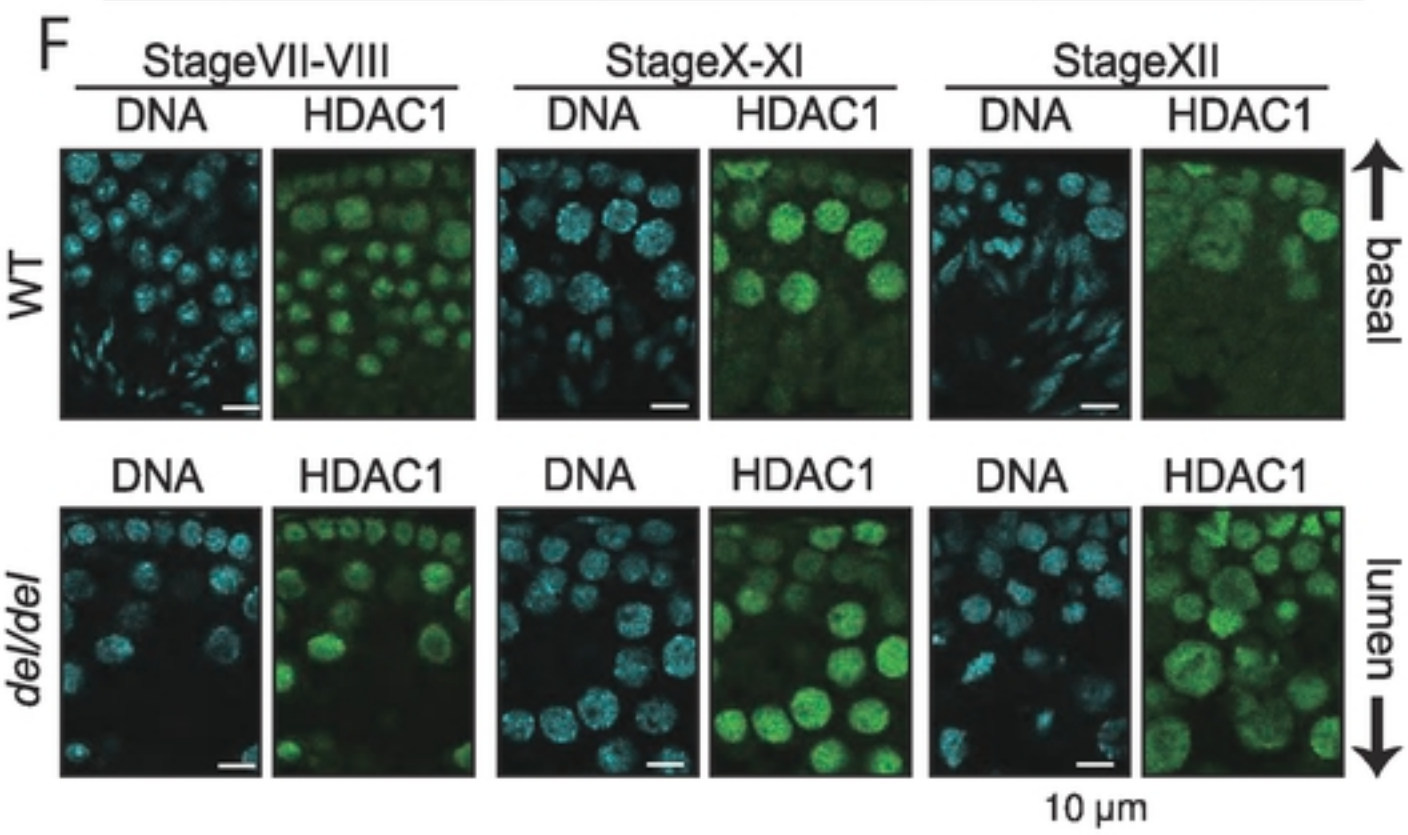

bioRxiv preprint doi: https://doi.org/10.1101/2021.02.12.430913; this version posted February 12, 2021. The copyright holder for this preprint (which was not certified by peer review) is the author/funder, who has granted bioRxiv a license to display the preprint in perpetuity. It is made available under aCC-BY 4.0 International license.

Figure6

bioRxiv preprint doi: https://doi.org/10.1101/2021.02.12.430913; this version posted February 12, 2021. The copyright holder for this preprint (which was not certified by peer review) is the author/funder, who has granted bioRxiv a license to display the preprint in perpetuity. It is made available under aCC-BY 4.0 International license.